# POLITECNICO DI MILANO

Facoltà di Ingegneria Civile, Ambientale e Territoriale

Master of Science in Civil Engeneering for Risk Mitigation

# Structural health monitoring of concrete dams: a review and a case study

Supervisor : Prof. Gabriella Bolzon

Author: Valerio Albertoni
Matricola : 876719

Academic Year 2018-2019

# Abstract

This thesis provides a literature review on the subject of Structural Health Monitoring (SHM) of existing concrete dams, with particular focus on the diagnosis of the behaviour of natural and artificial joints. Monitoring devices are introduced together with their basic principles and concepts. A case study is presented, in which a transient thermal analysis and a linear elastic static analysis of an arch-gravity dam with a large natural joint on the downstream face are performed. The simulation of this structural response aims to evidence the influence on measurable quantities of the presence and of the possible propagation of fractures in the dam subjected to the natural seasonal loading.

**Key words:** existing concrete dams; structural health monitoring; natural and artificial joints; thermal analysis; numerical simulation.

# Sommario

Questo lavoro di tesi fornisce una panoramica sulla letteratura presente in campo di monitoraggio strutturale di dighe in calcestruzzo, con particolare attenzione alla diagnosi del comportamento dei giunti naturali e artificiali. Oltre agli strumenti di monitoraggio e ai loro principi di funzionamento si presenta un caso studio, relativo ad una diga ad arco gravità con un vasto giunto naturale sulla facciata di valle. Il comportamento di questa struttura è simulato mediante analisi termica e strutturale statica, nell'ipotesi di comportamento elastico lineare del materiale. L'obiettivo di questa analisi è quello di evidenziare gli effetti della propagazione di una frattura sugli spostamenti indotti sulla diga dalle variazioni stagionali delle condizioni di esercizio.

**Parole chiave**: dighe in calcestruzzo; monitoraggio strutturale; giunti naturali e artificiali; analisi termica; simulazione numerica.

# Contents

# List of Figures and Tables

# 1. Introduction

In this thesis, the monitoring techniques currently utilised for the diagnosis of the behaviour of existing concrete dams are investigated. A particular attention is devoted to the behaviour of the dam joints. A case study is presented, in which the deformations of an arch-gravity dam with a large scale influential horizontal crack on the downstream face are studied under thermal loading.

## 1.1 Dams: general and structural characteristics

Dams are economically and socially important constructions, instrumental to irrigation of agricultural areas, water supplies for human communities, control of floods, navigation along rivers and non polluting production of renewable energy (Maier et al. [1]). If concrete dams are not well managed and maintained, failure might occur leading to life and economic losses. A variety of past events and ageing processes on concrete dams may imply concrete deterioration, which means loss of strength, stiffness and other physical properties of materials. According to the "International Commission on Large Dams" (ICOLD), although the overall failure rate of dams is around 1 %, a time-related analysis shows that this has been reduced by a factor of four or more over the last forty years. The improvement arises doubtlessly from the improvements in investigation techniques and from a wider dissemination of knowledge on risks.

Dams are hydraulic structures for damming a riverbed in order to raise the water level and to create an artificial lake called impounding reservoir (Tanchev [2]). They are built with local materials as clay, loam, sand, gravel, crushed stone, then concrete and reinforced concrete; particular structural elements require asphalt, steel, wood, plastic materials, etc. An enormous number of dams of various kinds have been built in the world, among which, the most widespread are embankment dams, then, various kinds of concrete dams. Embankment dams are erected by means of placement and compaction of local earthfill and rockfill materials. Their cross-section has the form of a trapezium and overflowing of water over this type of dam is not allowed. There can be different types of embankment dam. As first, homogenous embankment dams : the dam body is made of more or less

impervious material. As second, zoned embankment dams, with the presence of constructed zones of various materials in the dam body, where impermeability is ensured by means of a relatively thin zone of cohesive material. There is also a third type of embankment dam, the impermeability of which is achieved either by means of facing or by means of an internal core wall made of artificial material as concrete, reinforced concrete, asphalt, geosynthetics, or very rare steel.

Concrete dams are used for discharging the water from the impounding reservoir, since water-conveying and outlet structures can be carried relatively simply out in the dam wall. They are divided into gravity dams, buttress dams and arch dams. At a rough estimate, the cross-section of gravity dams has the form of a triangle and, as distinguished from embankment dams, they can be either constructed as no overflow dams or as overflow dams. A common feature of embankment and gravity dams is that horizontal forces are resisted by their self-weight, i.e. they act as gravity dams. Buttress dams consist of a relatively thin slab supported by buttresses on the downstream side. The foundation of arch dams has a curved form, with the convex side turned towards the water, whereas their cross-section is a relatively thin, curved wall. Upon the firm and sound rock, whereon arch dams are constructed, restrained arch girder are present, upon which horizontal loading are transmitted. Buttress and arch dams are also constructed as overflow dams, although much less frequently than the gravity dams are. In **Figure 1** , examples of embankment, gravity, buttress and arch dams are reported.

**Figure 1. "Tataragi"(JP) embankment dam (top left), "Mequinenza"(ES) gravity dam (top right), "Malga Bissina"(IT) buttress dam (bottom left), "Mauvoisin"(CH) arch dam (bottom right)**

Loadings acting upon dams are usually divided into primary, secondary, and exceptional loadings. Such a classification has been made depending on the probability of occurrence and the relative significance of the loadings. Primary loadings are of the utmost importance for all kinds of dams. To this class of loadings belong the forces from the hydrostatic pressure, the self weight of the structure, and forces due to seepage. Secondary loadings act on various kinds of dams, and have smaller magnitude than primary loadings, or else have a significant importance, but only for a certain type of dam. For example: loadings from sediment and ice; from the impact of the waves; from thermal effect and loadings from the interaction effect, namely internal loading caused by the relative stiffness, as well as differential deformations of the dam and its foundation. Another example of loading belonging to this class is the hydrostatic pressure in the banks: internal loading of seepage water on the rock mass in the banks, which is significant for arch dams. Exceptional loadings have been so named on the basis of their low probability of occurrence. Seismic forces belong to this group: horizontal and vertical inertial forces from the mass of the dam and the impounded water of the storage lake, originating from seismic influence.

As far as concrete dam joints are concerned, a distinction has to be made between natural and artificial joints. As of natural joints, concrete dams are likely to experience cracking due to the low tensile strength of concrete. Generally, concrete experiences a significant amount of hydration heat during cement hydration reactions, which starts immediately when cement is mixed with water. Though hydration heat is observed in all types of concrete, it can be particularly high in high performance concrete having low water-to-binder ratio. Hydration heat of cement can lead to surface breaking and formation of cracks. Another major cause for high hydration heat of concrete is the temperature of the surrounding environment. A high environment temperature leads to high placing temperature. The high placing temperature causes maximum temperature rise and leads temperature rising velocity of concrete at early ages. It increases the possibility of occurrence of cracks in concrete. Several concrete dams all over the world exhibited severe cracking phenomena among which horizontal cracks caused by internal and external temperature variations and shrinkage of the concrete are relatively common. The existence of the natural joints can endanger the serviceability of the structure. Cracks penetrating deep inside a dam may weaken its strength, rigidity, and impermeability. Hu and Wu [3] presented a statistical hydrostatic thermal-crack-time model to interpret displacements of concrete arch dams with

large scale horizontal cracks. The hydrostatic-thermal-crack-time model has been applied to analyze the “”Chencun” arch-gravity dam, presenting a large-scale horizontal crack on the downstream face, stretching horizontally across most of the dam blocks. A three dimensional “Finite Element” (FE) model, containing pre existing crack using special gap elements, has been built in order to reproduce the structural response of the dam and to obtain a relationship between the “Crack Mouth Opening Displacement” (CMOD) and the dam crest displacement. The obtained results showed that the crack and the corresponding reinforcement measure have a significant effect on the deformation behaviour of the dam. Regarding the reinforcement measure, the crack was treated using a modified epoxy resin. The measured crack mouth opening displacement values increased after the treatment up to a maximum value of 4mm. This is owing to the fact that grouting restricts the free closure of the crack under high temperature condition and makes the minimum CMOD values of most segments increase, equivalent to inserting a wedge at the crack tip. Grout injection is a crack repair technique commonly applied to deteriorated concrete structures. The grout resin is able to form a polymer plug sealing the crack, which aims at keeping out water, chlorides, carbon dioxide, sulfates, and other aggressive liquids and gases. Unfortunately, grouting is not effective for repairing the moving or influential cracks. This is because the materials are unable to act as a flexible joint material. Wieland and Kirchen [4] described the long-term monitoring of the “Punt dal Gall” arch dam. In particular, the cracks developed in the uppermost control gallery of the dam and are opening in winter and closing in summer when the concrete temperature near the dam crest is maximum. The cracks open by about 1.5 mm within one year.

Diagonal cracks are a further typology of natural joints and can form on abutments due to “Alkali-Aggregate-Reaction” (AAR) induced swelling of arch dams concrete. AAR is a slow and long lasting chemical reaction that produces mortar expansion and induces overstress status in the dam. The upwards swelling and bulging of the crest caused by AAR, combined with the constraints provided by foundations and abutments, results in diagonal shear cracks roughly parallel to the foundations. Human and Oosthuizen [5] described the rehabilitation works of the south african “Idas Valley” dam, discussing the observations of joints and postulating a possible future manifestations of the AAR swelling with its effects on the dam’s long-term behaviour. The widths of accessible cracks varied between 0.2 and 7 mm. A portion of the diagonal cracks developed on the right arch-abutment contact of the aforementioned dam are shown in **Figure 2**.

**Figure 2. Diagonal cracks on the right arch-abutment contact of "Idas Valley"(ZA) dam**

As of artificial joints, a further subdivision is made into construction and contraction joints. Construction joints are horizontal joints, provided for an easier, more systematic and economically convenient construction of the dam. They avoid excessive heat of hydration of cement, moreover the thickness of each layer of concrete should not be more than 1.5m in general and no more than 0.75 m for the first layer above the rock foundation. Construction joints are weak planes in the material, and their strengths depend strongly on the construction procedure and the materials employed. The properties of the joints may vary from one joint with a tensile strength very similar to that of the concrete to a joint that is a simple support of one concrete against the other, without any tensile strength. Campos et al. [6] presented hypotheses that could justify the high non-recoverable displacements of the "Mequinenza" gravity dam. In particular, the superposition of two effects has been assumed: a global phenomenon of water induced expansion in concrete in the entire dam and a localized effect consisting in the opening of cracks in the construction joints located in the

block containing the intake pipes and turbines. In 2006, the registered relative displacement between the aforementioned block and the adjacent block to the right in the downstream face reached the conspicuous value of 4.0 cm. A numerical analyses through 2D finite element models has been conducted, considering the nonlinear behaviour of the construction joints and using zero-thickness interface elements to simulate the potential cracking planes in the dam. The obtained results revealed the significant contribution of the opening of the cracks to the non-recoverable displacements in the dam.

Contraction joints are made to achieve necessary temperature control, to prevent cracks parallel to the length of the dam and to facilitate construction. They have to be able to transfer compressive and shear stresses. Hence, contraction joints should be grouted after cooling in order to create a monolithic block and be provided with suitable shear keys cast on the internal face of both the blocks. In particular, the spacing of transverse contraction joints shall be such as to suit the methods of construction, materials of the dam, the foundation conditions and the convenience of the location of outlets. Lin et al. [7] proposed a reasonable water level for smooth transverse contraction joint grouting during the filling process in "Xiluodu" double curvature arch dam, based on the effect of the reservoir water level on the aperture of the unsealed joints. The sealed region of the dam is the region where the transverse joints of the dam structure have been grouted using cement paste. In the first filling process, concrete placement in the dam structure and joint grouting are occurring simultaneously. The overall volume of the "Xiluodu" dam reservoir is as large as 12.67×109 $m^3$, thus there was the necessity to start impounding during the construction. The transverse joints are pressed tight due to the water load, which has a negative influence on the effectiveness of joint grouting. In order to avoid the joints being pressed too tight, the authors concluded that the water level should be 30 to 40m below the top of the dam's sealed region based on the numerical simulation. The peak values of a reported example of transverse joints aperture are about 5mm. The numerical modelling has been conducted by a three-dimensional nonlinear finite element method, taking the nonlinear contact of the transverse joints between dam monoliths into account. As an example of transverse contraction joint, **Figure 3** presents the joint in the upstream face of "Mequinenza" gravity dam.

**Figure 3. Transverse contraction joint in the upstream face of "Mequinenza"(ES) gravity dam**

For large structures the problems of cooling large masses of concrete are conspicuous. One of the measures used to control cracks parallel to the length of the dam in case of high dams is to subdivide the monolith into several blocks by longitudinal contraction joints and subsequently grout these joints to ensure monolithic action. The spacing of longitudinal joints is largely dictated by convenience of construction and foundation conditions. Cui et al. [8] carried out a numerical simulations with 3D nonlinear FE model of the construction period, the grouting process and the operation period of the "Three Gorges" gravity dam, in order to understand the contact condition of longitudinal joints and the influence on the dam body stress. In the construction process of the dam, two longitudinal joints are set according to the need of temperature control. The two longitudinal joints are 25.0m, 69.7m away from the upstream surface separately and divide the dam into three parts: up, middle and down. The achieved results showed that the opening of the longitudinal joint varies with year temperature, water cooling, water load on the upstream surface as well as with the construction process. Moreover, it has been shown that the reopening of the longitudinal joints after grouting is mainly due to the deformation of the dam body, caused by the annual variation of temperature: the joints opening

being in the worse case less than 2mm. On the other hand, the carried out computations demonstrate that the current contact condition of longitudinal joint has little effect to the vertical stress of dam heel. Eventually, it has been suggested that secondary grouting to the longitudinal joint may not be carried temporarily and that the monitoring to the variation of the longitudinal joint should be strengthened.

## 1.2 Diagnosis tests and monitoring activities

As far as the diagnosis of concrete dams is concerned, dynamic and static properties of the dam under study are determined through dynamic and static tests, respectively. Dynamic tests facilitate the estimation of modal parameters as resonant frequencies, damping ratio and mode shapes. The behaviour of dams under vibrations can be tested by either Forced Vibration Testing (FVT) or by Ambient Vibration Testing (AVT). In the forced vibration tests, dams are excited by mechanical means using shakers (i.e. eccentric-mass shaker located at several position along the crest of the dam) and the vibration responses are measured by accelerometers. With the force signal acting as a reference to all response signals, dynamic properties of the dam are extracted using Frequency Response Functions (FRFs). Signals along the whole crest of the dam can be measured and the identified modal properties of the Dam-Reservoir-Foundation (DRF) system can be used as a basis for the calibration of a FE model. However, due to accessibility issues of the areas where dams are located, the transportation of the mechanical exciters to site becomes very complicated and expensive. AVT represents a practical way of carrying out dynamic tests on dams. In ambient vibration testing only responses from the structure are measured and it uses environmental forces (wind, ground motion) to excite the structure. Instead of using the force signal as a reference, the response signal measured at one or more points is used while estimating the dynamic properties. Nevertheless, in dam engineering the results of dynamic tests (both FVT and AVT) can be significantly influenced by factors as: fluid–structure interaction, which can significantly change natural frequencies and mode shapes; foundation deformability and non-linear behaviour of natural and artificial joints. Moreover, there is an issue related to the difficulties in extending results of FVT to the response of dams under seismic excitations, that are likely to lead to a non-linear behaviour of parts of the dam.
Static monitoring of dams involves measurement of static factors such as ambient temperatures, reservoir level, opening and closing of joints, displacements and strains which are measured accurately by instruments

(Bukenya [9]). Regarding the external action due to the hydrostatic load, the static test starts from an initial situation of full reservoir; the water level is then decreased from the maximum to the minimum storage, in order to induce as large as possible displacements in the dam. This can be obtained either in a few days by discharging the stored water through all the outlet devices, or by exploiting a seasonal oscillation between extreme service levels that are more or less close to the maximum and minimum values. The hypothesis of short-term experiment, in the static analysis, allows not to take thermal effects into account. Exploiting static excitation for diagnostic purposes, many of the drawbacks of the modal approach are avoided. In particular, the static approach is well suited for non-linear problems. As far as the static characterisation of concrete dams is concerned, both stochastic analysis and structural identification through inverse analysis as well as deterministic analysis can be performed. The purpose of statistical models, supported by monitoring and inspection activities, is to predict the behaviour of concrete dams or to assess the consequences of significant deviations. The most popular data-based approach for dam monitoring analysis is the hydrostatic-season-time (HST) model. It was first proposed by Willm and Beaujoint [10] to predict displacements in concrete dams and it has since been widely used for analyzing monitoring data of concrete dams. The HST model is based on the assumption that displacements are associated mainly with three factors: hydrostatic loads, external temperatures (air and water), and time effects. Another common choice is to replace the periodic function of the thermal component in the HST model by the actual temperature in the dam body, resulting in the hydrostatic-thermal-time (HTT) model. However, under certain circumstances the deformations in a dam may not be explained only by these traditional causes. Concrete dam behaviour is also dependent on material and geometrical properties of the foundation and the dam itself and the reinforcement measures during operation. A limitation of the original forms of the HST and HTT models is that geometrical variation and structural reinforcement measure are not considered. It reduces its prediction accuracy for dams suffering serious cracks or experiencing reinforcement measures.
Through inverse analysis the best-fitting unknown structural parameters are sought, for instance, on the basis of the generalized least square (GLS) formulation by minimizing a discrepancy function between measured data and computed data. Eventually, deterministic models establish the relationship between the loads and the dam response, defined by structural analysis. Both the three aforementioned procedures can be useful in anticipating the structural response (i.e. upstream– downstream crest

displacements) of concrete dams. Some difficulties can arise in the case of static tests due to the fact that the static load could be not sufficient to properly excite the structure and the monitoring system could provide not enough information for the solution of the inverse problems. However, if large dams are considered, considerable static loads are available (for example by change of reservoir water level) and there is the possibility of an effective application of static damage diagnosis (Maier et al. [1]).

The activities and instruments which can be taken into account to supervise the "health" of an existing infrastructure, such a dam, are commonly defined with the term "Structural Health Monitoring" (SHM).
The older procedure for evaluating the structural integrity of dams is through visual inspections. Visual inspections are conducted by experienced engineers in order to recommend actions to be carried out on dams under inspections and to solve the identified problems. Visual inspection is usually supplemented by displacement transducers like pendulums and collimators. Pendulums can measure relative displacements between two points on the same vertical straight line with high precision, namely ±0.05 mm (Maier et al. [1]). Collimators measure absolute displacements, in the horizontal direction along the line of sight with an error of about 0.5 mm. As of natural and artificial joints monitoring, instruments embedded in the structure can be used for joints opening displacement measurements. In particular, fibre-optic sensors, vibrating wire crack meters as well as 3-D crack gauges can be used to monitor movement across cracks and joints surfaces. Ground-Based radar Interferometry with Synthetic Aperture Radar (GB InSAR) technique is also used with the aim of determining the deformations of dams. Large number of points can be monitored by these remotely sensed tools, which do not require targets to be positioned on the structure and can estimate displacements with an absolute error of about ±0.25 mm (Ardito and Cocchetti [23]). Another monitoring technique that can be used for the SHM of concrete dams is Terrestrial Laser Scanning (TLS), which can get the coordinates of millions of points in reflecting surfaces thus providing new means for rapid and precise geometric, discrete but very dense, electronic representation of objects (Berberan et al. [11]). TLS allows to capture dense clouds of unspecific points in 3-D with a high degree of automation, although with a poor accuracy for deformation measurement (Alba et al. [12]).
Recently, a great deal of attention has been aroused by the opportunity to measure displacement, strain, and dynamic parameters of structures using optical techniques and digital cameras. An example of optically based

technique is 3D Digital Image Correlation (DIC). The basic principle of DIC is to match the same physical point between a reference image and several deformed stages based on gray-scale variations of continuous patterns. Long-term monitoring of concrete dams can be performed by Unmanned Aerial Vehicles (UAVs) and DIC technologies combined together. UAVs are small-sized aircrafts, which can fly autonomously, controlled remotely either by computers or by trained personnel.

# 2. Monitoring techniques

In the course of construction and particularly during the service period, it is necessary to perform continuous monitoring and surveillance of the concrete dam in order to have permanent insight into the condition and behaviour of the structure, enabling timely anticipation of any possible threat to its safety (Tanchev [2]).

In the case of concrete dams, the temperature in the dam body, strains and deformations, opening of joints, stresses as well as the uplift pressure of pore water, filtrated into the concrete and the foundation are kept under observation. The measurements of air, water and structure temperatures are carried out in order to study the consequences of thermal effects in the diagnostic analysis. However, if the relevant hydro-static loading occurs in a few days, thermal effects can be disregarded.

When deploying monitoring devices, the location and the abundance of the instruments as well as the frequency of readings need to be addressed. Regarding the location of the instruments, the monitoring should encompass the zones with maximum expected values of stresses, deformations, and points at which they have previously been calculated, in order for it to be possible to carry out comparisons of the expected values and the actual ones. The abundance of the instruments depends on the type, size, and complexity of the structure that is under observation. Higher and more complex structures require more instruments. For instance, in the case of arch dams, as more sophisticated and more sensitive structures, it is necessary to perform more complex surveillance, in comparison with gravity dams and buttress dams. The sampling frequency depends upon the risk derived from the presence of the structure on the territory, the typology of the structure and the magnitude and rapidity of its movements. The singularities of each structure and of the surrounding environment make impossible the application of standards for periodicity, except for some general guidelines (Giussani [13]). Typically, the sampling frequency varies during the service life of a dam. The frequency is usually higher during the first fill- up of the reservoir and decreases with the number of years of service life. (Chouinard and Roy [14]).

Another issue of particular importance is the selection of appropriate equipment and its proper installation at critical locations. The selection of the monitoring device to be used depends on the type of movement to be monitored and the required accuracy, which has to be smaller than the

movement itself. Displacements are measured with respect to a reference point that can be external to the structure (absolute displacements) or belonging to the structure in a mutual and not next position (relative displacements). Absolute and relative displacements of concrete dams can be measured by means of plumb lines, tangent line collimation and precise levelling. Moreover, measurements of the rotation of some reference axis in relation to certain horizontal or vertical planes are performed at selected places in the galleries of concrete dams, by means of clinometers and inclinometers. Instruments embedded in the structure can be used for joints opening displacement measurements. Special methods can be also be utilised for concrete dams structural health monitoring: Ground-Based radar Interferometry with Synthetic Aperture Radar (GB InSAR) technique, Terrestrial Laser Scanning (TLS) and Digital Image Correlation (DIC).

## 2.1 Visual inspection and traditional instruments

The traditional procedure for evaluating the structural integrity of dams is through visual inspections. Visual inspections are conducted by experienced engineers in order to recommend actions to be carried out on dams under inspections and to solve the identified problems. The measurement processes is fundamentally simple, however, it is highly subjective and it focuses on the observation of very few details at a time. The inaccessibility of critical parts of the structure under surveillance represents an additional drawback. For instance, damages in the upstream side, developed under the water level or in correspondence to the contact between dam and foundation rock cannot be detected. Large scale deformations and internal damages are also particularly difficult to diagnose. Furthermore, the collected information is often inaccurate from a positional point of view, making the outcome of visual inspections positionnally inaccurate (Berberan et al. [11]). However, visual inspection can be improved by the use of Unmanned Aerial Vehicle (UAV) equipped with a camera. UAVs are small-sized aircrafts, which can fly autonomously, controlled remotely either by computers or by trained personnel. Initially developed for military operations, in the last years they found applications in civil scenarios as well. Among them, flora and fauna monitoring, environmental disaster management, and heritage documentation. Kaamin et al. [15] used Unmanned Aerial Vehicle in order to perform a visual inspection of the exterior structure of “Perak Museum”. According to the authors, this technology offers the possibility to quickly

map the different areas with high flexibility. The inspection methodology followed the following steps: planning and preparation, data collection using UAV, image processing and data analysis.

As of planning and preparation, the distance between UAV and building must be set as well as the direction of flight, which is made by vertical and horizontal paths (**Figure 4**).

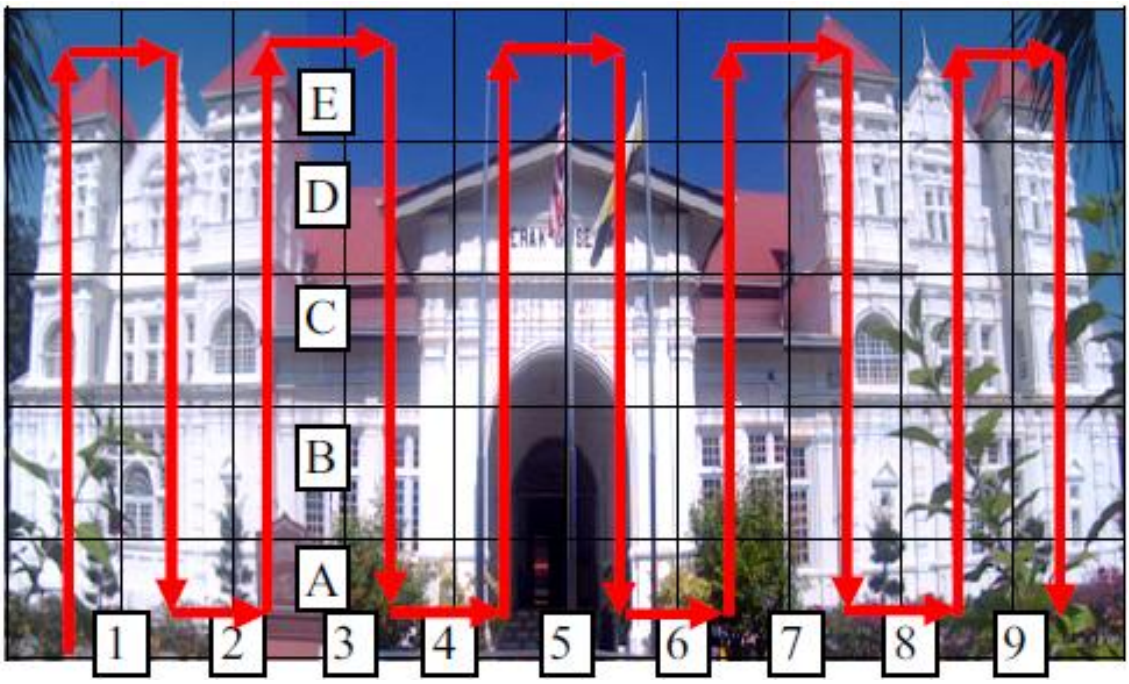


**Figure 4. Flight direction**

The authors concluded that the methodology is able to show in details the defects of the exterior structure of the building together with their severity. Moreover, the use of UAV in the inspection of historical buildings can help minimizing costs and time of operations.

Pendulums are among the most used displacement transducers in concrete dam engineering. There are cases of hollow buttress gravity dams, built in the 1950's, for which records of the upstream–downstream crest displacements, measured with a high degree of accuracy by direct pendulum devices, span over 40 years (De Sortis and Paoliani [16]).
Pendulums measure in-plane relative displacements between two points of the dam placed on the same vertical line, or between a point belonging to the dam and another located in the foundation, with high precision, namely ±0.05 mm (Fedele et al. [17]). They are positioned inside the dam in ad hoc vertical tunnels, the number and location of which have been selected in the

design process. Direct and reverse pendulums are used. A direct pendulum is composed of a steel wire anchored in the upper part of the structure, ballasted at the bottom by a proper weight that can move inside a tank filled with a damping fluid. The relative horizontal displacements are measured between the anchoring point and the detecting point of the wire, e.g., along upstream downstream and right–left directions. Reverse pendulum works according to the same concept, but the wire anchorage is on the bottom part, generally inside a bore-hole in a non-accessible location, e.g., in the dam foundation. The measurements are performed at measuring stations, located in horizontal openings at various levels of the dam, in order to obtain a deflection along its entire height. They are performed by means of a sliding micrometer, provided either with a peep sight or with a microscope, set up in the measuring stations. **Figure 5** shows a schematic representation of a direct pendulum.

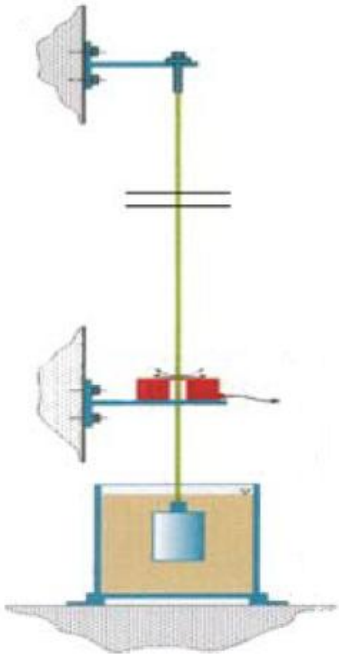

**Figure 5. Schematic representation of a direct pendulum**

The installation of a plumbline is very often used in gravity dams, as well as in arch-gravity dams.

Collimators measure the absolute displacements of some selected points of the dam crest, orthogonal to the straight line between two fixed reference points on the rocky slopes near the dam abutments, with an error of about ±0.5 mm (Fedele et al. [17]). For each monitoring point on the dam crest, the horizontal displacement component can be measured perpendicularly to the

dam profile. Three to four measuring points are usually located, and the results are combined with the results obtained from measurements by means of a plumbline. **Figure 6** shows a schematic representation of a collimator.

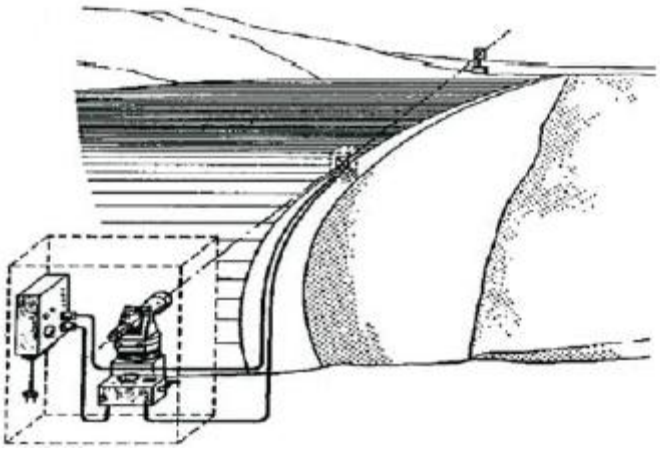

**Figure 6. Schematic representation of a collimator**

An example of combination of collimators and pendulums is provided by the monitoring system of the "Pian Telessio" arch-gravity dam . The dam, which had been chosen as a case study for the "Theme A" of the 2001 ICOLD benchmark, is equipped with plumb-lines on four vertical sections and with three optical collimators. (**Figure 7).**

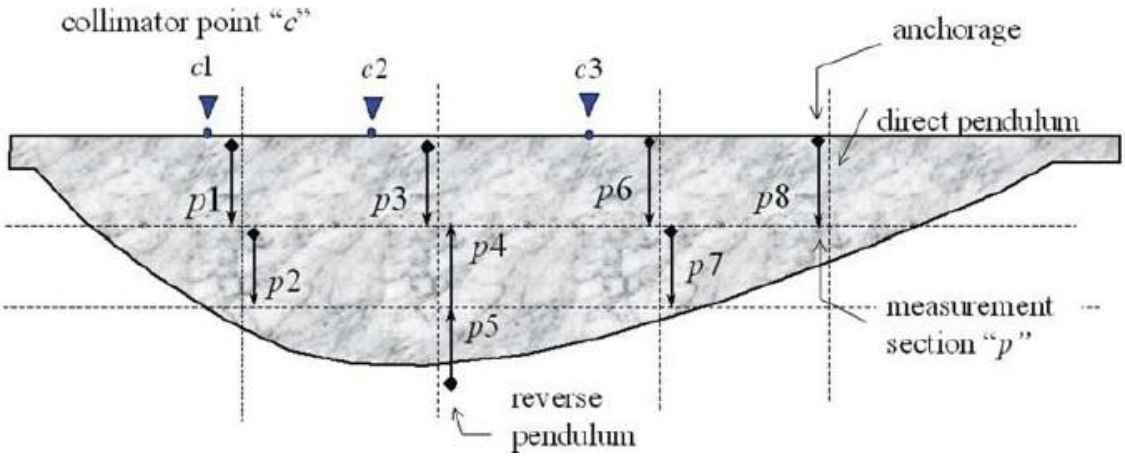


**Figure 7. Collimators and plumb lines locations in the "Pian Telessio" arch-gravity dam**

More abundant data for displacements are obtained by means of triangulation measurements. For that purpose, a system of triangulation targets is placed on the surface of the dam, namely on crest, downstream face, as well as on appurtenant structures. This system requires a net of

instrument piers and a base line downstream of the dam. **Figure 8** shows a scheme of layout of triangulation measurement on a concrete dam (Tanchev [2]).

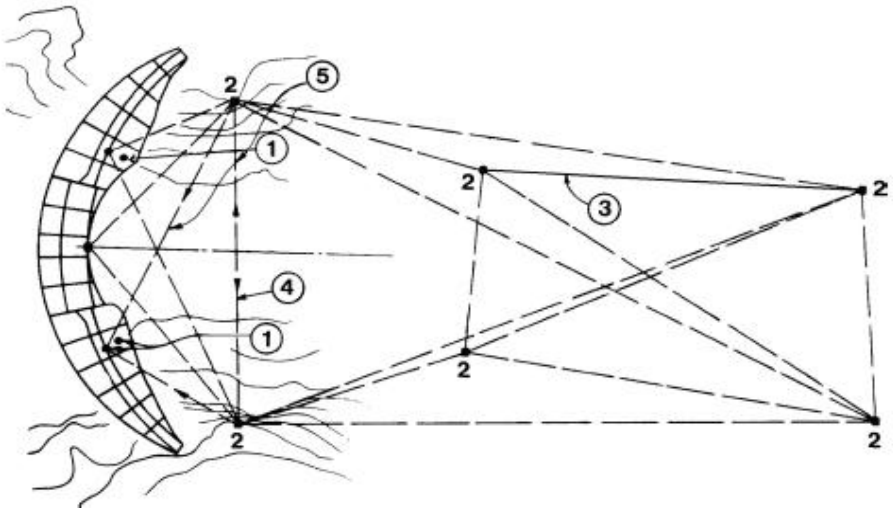


**Figure 8. Scheme of layout for triangulation measurement**

In particular, in **Figure 8** measuring targets on the dam surface (1), measured (3) and computed (4) base lines, as well as sight lines (5) are shown. The instrument piers (2) should be positioned so as to make possible collimation from each pier to as many measuring targets as possible. The number of piers is dictated by the nature and topography of the surrounding ground. The results of triangulation measurements are deformations of the dam, in relation to the targets outside its body, and deformations of the canyon downstream of the dam, in the direction of the river flow and perpendicular to it.

Levelling measurements serve for the determination of vertical displacements of points of the structure in relation to off-dam references, positioned sufficiently far away from the zone in which we can expect settlements caused by the structures of the hydraulic scheme, as well as the water in the reservoir. Similarly to triangulation measurements, levelling measurements also require the use of precise instruments and methods.

At some concrete dams, measurements of the rotation of some reference axis in relation to certain horizontal or vertical planes are carried out. Such measurements are performed at selected places in the galleries, by means of clinometers and inclinometers. Clinometers, used for measuring changes of the angles in relation to the horizontal plane, are more often employed than inclinometers, used for measuring the angle of rotation in relation to the

vertical. In the case of arch dams, especially of double-curvature arch dams, the execution of a vertical well for a plumbline is usually not possible. The installation of clinometers can be a solution to this problem. (Tanchev [2]).

## 2.2 Embedded instruments for joints opening measurements

A lot of surveillance instruments are produced in the world, intended for embedding in the body of concrete dams (Tanchev [2]). For the purpose of this study, the following have been investigated: fibre-optic sensors, vibrating wire crack meters and 3-D crack gauges.

Fibre-optic measurement systems emit light into glass fibres and analyse the returning signal. The light source and the signal analyser are usually integrated in one instrument called reading unit. In a quasi-distributed system, sensors are physically placed at the desired measurement locations. These systems use Fibre Bragg Gratings (FBG) which are periodic refractive index changes inscribed into the fibre. With quasi-distributed fibre-optic sensors it is therefore possible to obtain measurements at many points along the fibre-optic cable. **Figure 9** shows the functioning principle of FGB (Lienhart et al. [18]).

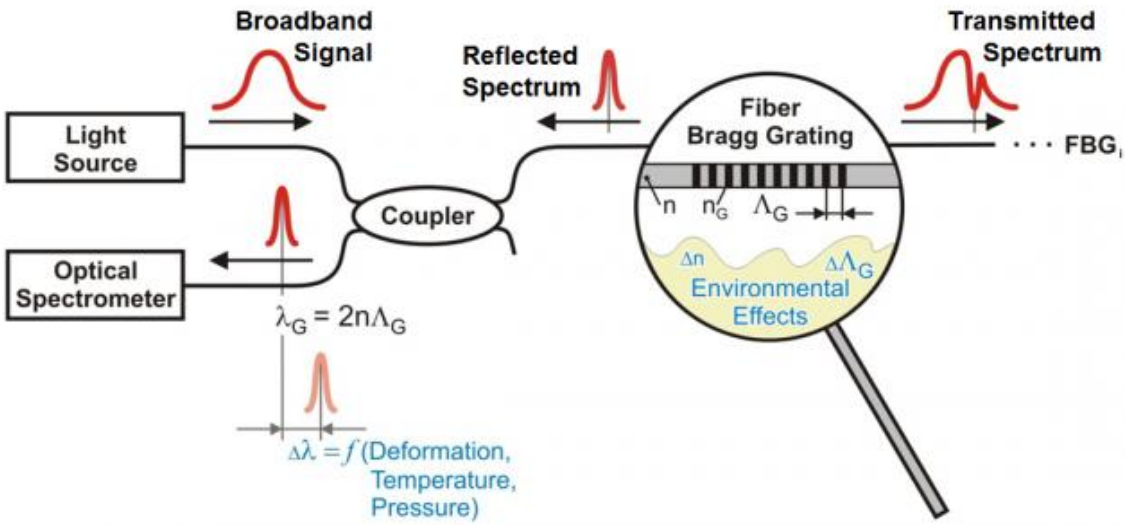


**Figure 9. Transmitted and reflected spectrum of an FBG**

Light with the Bragg wavelength gets reflected at the position of the grating. This reflected signal can be measured with an optical spectrometer. When the length of the FBG changes, the spacing of the grid also changes and thus the reflected wavelength shifts. This wavelength shift can be

measured and converted into length changes. An FBG follows the deformations of the object if the cable is fixed to the monitoring object on both sides of the FBG. In this case an elongation or shortening of the distance between the fixation points results in FBG wavelength shifts which can be measured and converted into strain values. Lienhart et al. [18] studied the installation of a quasi-distributed fibre-optic sensors system in one of the inspection corridors of the Austrian "Kops" arch-gravity dam. In particular, 15 transverse contraction joints were equipped with FBG sensors. **Figure 10** shows the "Kops" arch-gravity dam together with the locations of the fibre-optic cables and sensors located in one of the inspection corridors.

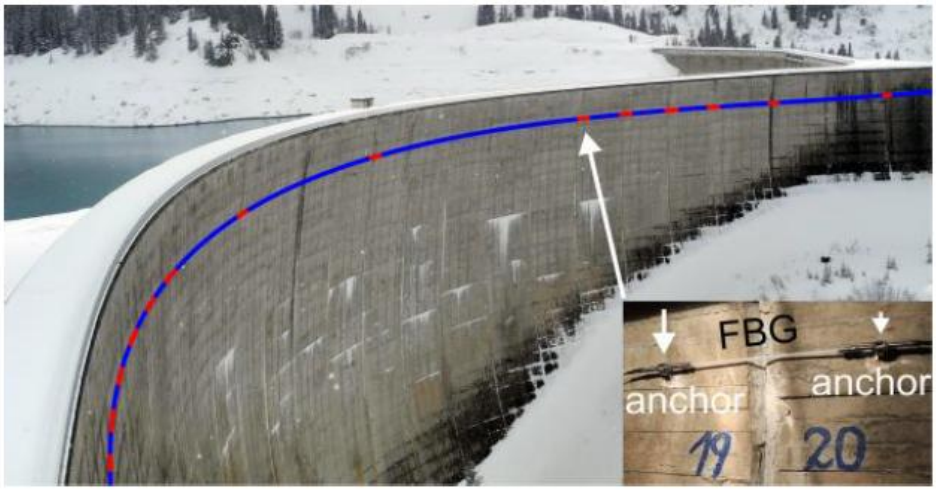


**Figure 10. Fibre-optic cable (blue) and sensors (red) located in one inspection corridor**

Metal anchors at each end of the sensor ensured a rigid connection to the concrete dam and therefore the cable could be used to measure length changes of the contraction joints. Achievable accuracies were in the range of 1με, corresponding to 1μm with a distance between the fixation points of 1m. With a distance of 40cm between the anchor points, 0.4 μm precision is achievable, with maximum contraction joint movements of about 3mm, known from previous measurements.

Vibrating wire crack meters are used to measure movements across natural and artificial joints in concrete dams. They are installed by grouting, bolting, bonding or fixing expandable anchors to either side of a joint to be monitored. A variation in distance between the anchors caused by the joint opening or closing changes the tension on the vibrating wire, altering the resonant frequency of the wire. The latter frequency of vibration is measured by the use of a magnetic circuit. The measurements can be made

by electrical readouts (www.geosense.co.uk [19]). **Figure 11** shows a schematic representation of a vibrating wire instrument (Thanchev [2]).

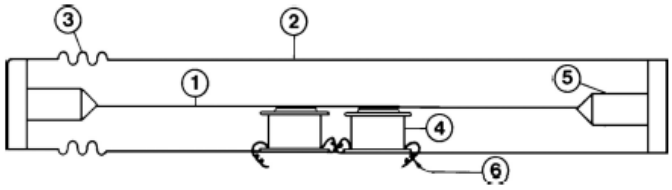


**Figure 11. Scheme of vibrating wire instrument: (1) vibrating wire; (2) case; (3) bellows; (4) electric magnet; (5) cuck; (6) lead.**

3-D crack gauges allows the natural joints opening displacements to be measured. They consist of two plates overlapping for a part of their length. The bottom plate is calibrated in millimeters and the top plate is transparent and marked with a cross shaped cursor. If the joint opens or closes the cursor moves relative to the calibration scale (www.berntsen.com [20]). The readings can be manually recorded with digital callipers (**Figure 12**).


**Figure 12. Joint opening measurement with 3-D crack gauge and digital caliper**

An accuracy of measurements in the x (across the crack or tangential direction), y (vertical), and z (radial) directions of 0.02mm can be achieved. 3-D crack gauges are fixed across the joints using screws and plugs or adhesive. Prins [21] investigated the three dimensional crack width gauges located on the downstream face and the gallery of the "Kouga" dam. In particular, two periods were investigated, in order to observe the impacts of rising and falling water level on the transverse contraction joints of the structure. The first period was characterised by falling water level and the maximum opening of joints, measured by 3-D crack width gauges, was approximately 1 mm. The measurements showed that the largest joint movements for both periods occur in the middle of the structure and that

the joints are more open during low water levels. On the other hand, when the water level was higher the joints were more closed, with the dam wall in a more compressed state. Crack width gauge results for the displacement across the joints (tangential) for the second period (rising water level) are shown in **Figure 13**. Values highlighted in green indicate a opening of the joint while those highlighted in red/orange indicate a closure of the joint. The yellow values indicate little change in joint movement.

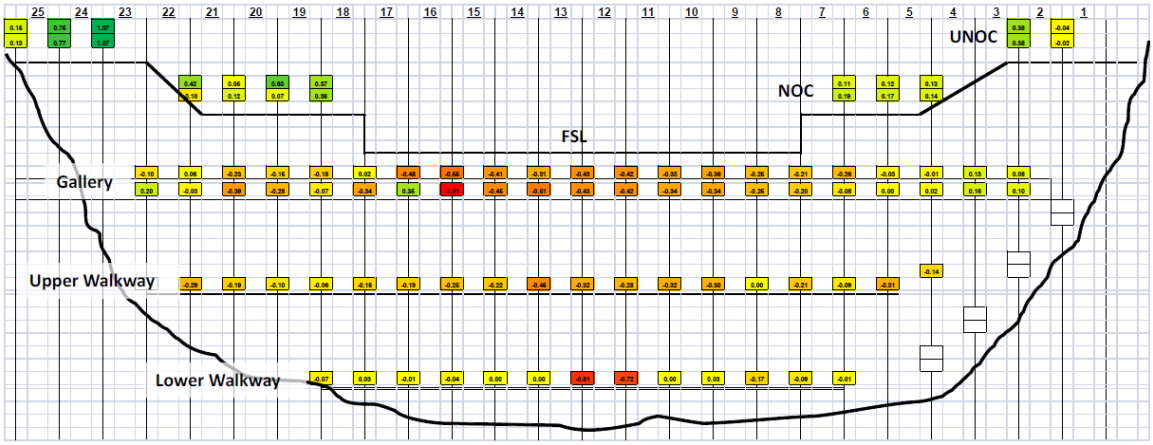


**Figure 13. Displacement across the joints (tangential) for the second period (rising water level)**

## 2.3 GB InSAR and TLS

Ground-based interferometry with Sinthetic Aperture Radar (GB InSAR) technique is playing an increasingly important role in determining the deformations of dams. In particular, the three techniques applied by the instrument are: Stepped Frequency Continous Wave (SF-CW), Synthetic Aperture Radar (SAR) and Interferometry (Talich [22]). The SF-CW technique provides the system with range resolution capability exploiting the duality between time and frequency domains: a burst of N monochromatic pulses equally and incrementally spaced in frequency are transmitted. By taking the Inverse Discrete Fourier Transform (IDFT) of the samples acquired in the frequency domain, the response is reconstructed in the time domain of the radar. The amplitude range profile of the radar echoes is then obtained by calculating the amplitude of each sample of the IDFT of the acquired vector samples. The latter range profile gives a one dimensional map of scattering objects in the viewable space in function of their relative distance from the equipment (Alba et al. [12]). The illuminated area is divided into circular segments (resolution cells) of constant distance

from the radar and the width of the segments is called range resolution ΔR (**Figure 14).**

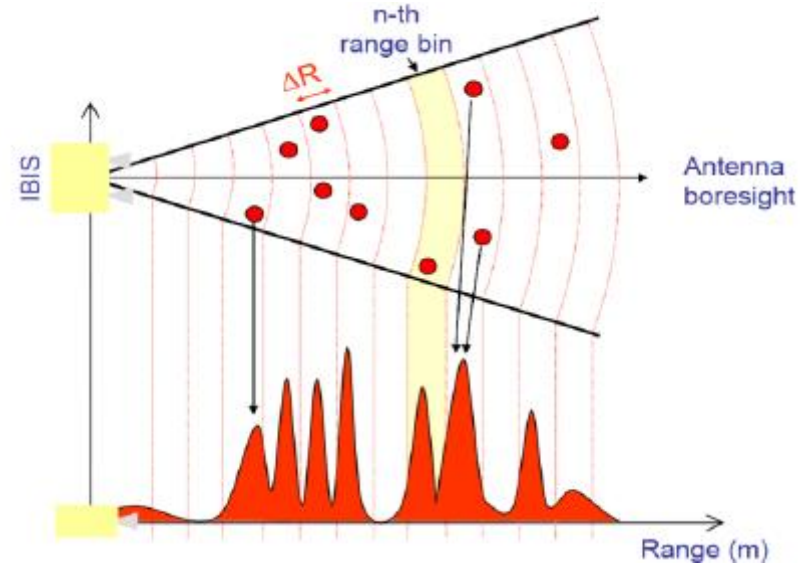


**Figure 14. Graphical representation of range resolution**

SAR uses multiple acquisitions of given scene from separate positions to refine the cross-range resolution. The multiple acquisitions are achieved by moving the radar along a rail. **Figure 15** shows the radar on its rail used for the monitoring of the "Cancano" dam (Alba et al. [12]).

**Figure 15. Radar positioned in front of the downstream face of "Cancano"(IT) dam**

The combination of the SF-CW technique with the SAR technique leads to the radar image being organized into pixels. For each of these pixels both amplitude (a characteristic of reflectivity) and phase (characteristic of distance) of returned signal are known. The phase is used in computing movements.

Interferometry allows the displacement of a scattering object to be evaluated by comparing the phase information of the electromagnetic waves reflected by the object in different time instants. The Line-of-Sight displacement ($d_{LoS}$) of the investigated object is determined from the phase shift measured by the radar sensor at the discrete acquisition times. (**Figure 16**)

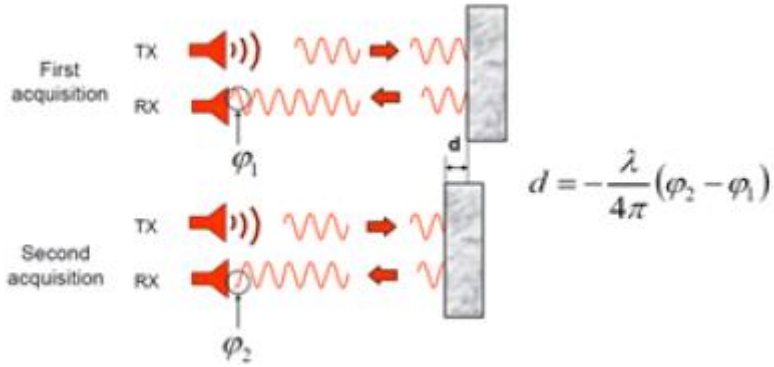


**Figure 16. Graphical scheme of the radar interferometry principle**

Once $d_{LoS}$ has been evaluated, the vertical and horizontal displacements can be found by making geometric considerations.
Remotely sensed measurements of a great number of points are carried out by the use of GB InSAR technology and there is no need of targets to be positioned on the monitored structure. Moreover, the precision of the achieved measurements is independent from the weather conditions as well as from the lightening. The displacements of a structure can be estimated with an absolute error of about ±0.25 mm (Ardito and Cocchetti [23]). On the other hand, some drawbacks and limitations must be pointed out. Only displacement projection along the line of sight can be measured and displacement maps are strongly influenced by the reflectivity characteristics of the monitored object or by movement of loose parts (wiring, railing, lamps, etc.).

Terrestrial Laser Scanning (TLS) can get the coordinates of millions of points in reflecting surfaces thus providing new means for rapid and precise geometric, discrete but very dense, electronic representation of objects (Berberan et al. [11]). TLS allows to capture dense clouds of unspecific points in 3-D with a high degree of automation, although with a poor accuracy for deformation measurement (Alba et al. [12]). The application of the GBInSAR technique to the arch gravity dam of Cancano lake by Alba et al. [12] addresses the monitoring of the displacement of the dam due to an increasing load of the water basin during two days and to temperature change. The integration between Terrestrial Laser Scanning (TLS) and

GBInSAR pointed out that TLS is able to detect lower frequency deformations with a higher point density, while the GBInSAR is capable to monitor higher frequency at a lower spatial resolution. The latter is a point of strength GBInSAR technique in case of constructions like dams, featuring large regular surfaces, where a huge point density is not a key issue, like the accuracy is. According to the authors, TLS can be used to evaluate seasonal deformations of structures with points featuring displacements of a few centimetres, but not for the continuous monitoring.

## 2.4 Digital Image Correlation

Recently, a great deal of attention has been aroused by the opportunity to measure displacements and strains using optical techniques and digital cameras. An example of optically based technique is Digital Image Correlation (DIC). DIC is an effective and flexible optical technique for surface deformation measurement from the macroscopic to micro- or even nanoscale. The basic principle of DIC is to match the same physical point between a reference image and several deformed stages based on gray scale variations of continuous patterns. Thus, to perform DIC measurements, a stochastic pattern made of black and white dots or optical targets is applied to the targeted surface. Then, the relative position of each dot is tracked as the surface deforms over time. In each of the measuring areas, a set of unique correlation point is defined, whose position is tracked through each of the successive acquired images (Reagan et al. [25]).

In particular, the implementation of the 2D DIC method comprises the following three consecutive steps: specimen and experimental preparations; recording images of the planar specimen surface before and after loading; processing the acquired images using a computer program to obtain the desired displacement and strain information (Pan et al. [24]). In the 2D DIC method implementation, the region of interest (ROI) in the reference image should be defined at first, which is further divided into evenly spaced virtual grids. The displacements are computed at each point of the virtual grids to obtain the full field deformation. The basic principle of 2D DIC is the tracking of the same points between the two images recorded before and after deformation. In order to compute the displacements of a point P, a square reference subset, centred at point P(x0, y0) from the reference image, is chosen and used to track its corresponding location in the deformed image. A square subset, rather than an individual pixel, is selected because

the subset comprises a wider variation in gray levels and it can be more uniquely identified in the deformed image. To evaluate the similarity degree between the reference subset and the deformed subset, a Cross Correlation (CC) criterion or Sum Squared Difference (SSD) correlation criterion must be predefined. The matching procedure is completed through searching the peak position of the distribution of correlation coefficient. Once the correlation coefficient peak is detected, the position of the deformed subset is determined. The differences in the positions of the reference subset centre and the target subset centre yield the in plane displacement vector at point P (**Figure 17**) (Pan et al. [24]).

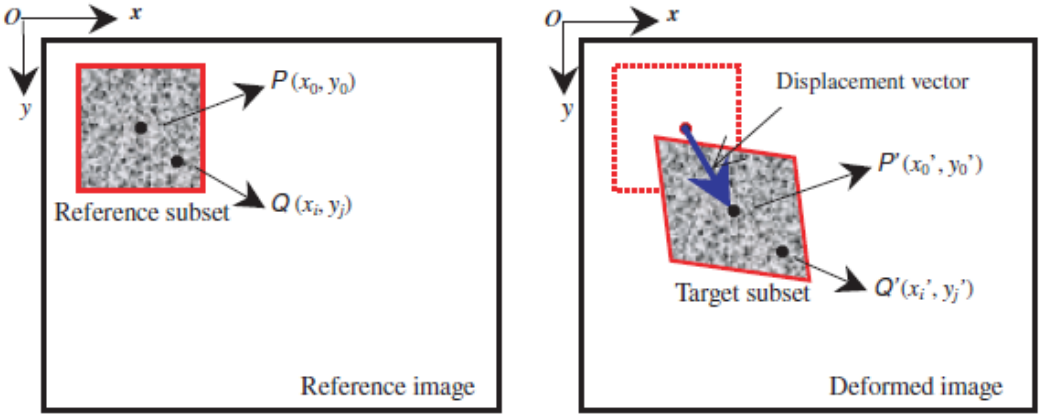


**Figure 17. Reference square subset before deformation and deformed subset**

Some requirements must be met, in order to correctly implement the 2D DIC method. The specimen surface must be flat and remain in the same plane parallel to the sensor target during loading. This implies that the sensor and the object surface should be parallel, and out of plane motion of the specimen during loading should be small enough to be neglected. The out of plane motion of the specimen leads to a change in magnification of the recorded images, which further yields additional in plane displacements. Thus, it should be avoided for accurate displacement estimation. Normally, the out of plane motion can be somewhat alleviated by placing the camera far from the specimen. Furthermore, the imaging system should not suffer from geometric distortion. In an optical imaging system, geometric distortion impairs the ideal linear correspondence between the physical point and imaged point and produces additional displacements. If the influence of geometric distortion cannot be neglected, corresponding distortion correction techniques should be used to remove the influence of distortion to provide accurate measurements.

2D DIC can only be used for in plane deformation of a planar object. Therefore, for deformation measurement of a macroscopic object such as

structural components, the advanced 3D DIC is more practical and effective because it can be used for the 3D profile and deformation measurement of both planar and curved surfaces, and is insensitive to out of plane displacement. 3D DIC has become a valuable asset for performing non contact measurements and extracting surface strain, displacement and geometry profiles from images acquired through a synchronized pair of stereo cameras. For the sake of performing long term monitoring of concrete dams Unmanned Aerial Vehicles (UAVs) and DIC technologies can be combined together. Reagan et al. [25] proposed an approach that combines the use of unmanned aerial vehicle (UAV) and 3D-DIC to perform remote monitoring of concrete bridges' cracks, by using a pair of cameras installed on a UAV payload. A trained pilot remotely controlled the UAV, namely, the UAV was operated independently from the DIC sensor payload. The UAV operator positioned and maintained the vehicle relative to the patterned areas of interest as instructed by the DIC payload operator. A camera installed underneath the payload allowed the operator to see the surface the UAV was flying over. Once the DIC operator was satisfied with the positioning of the UAV, images could be acquired and the aircraft could be repositioned to the next local inspection area. Two monitoring activities have been performed over a currently in service, 56 years old, concrete bridge, in particular, two different locations in correspondence of two contraction joints on the bridge's abutment walls right below the bridge's superstructure have been monitored. **Figure 18** shows the area of interest of the first monitored location, which is across the expansion joint and it also shows the applied stochastic pattern with black dots.

**Figure 18. UAV inspection at the expansion joint on the bridge's abutment wall**

Data was collected by measuring the changes in relative position between optical targets placed across the expansion joint. The centre of each optical target was a measurement point that can be thought of as the edge of an extensometer. The position of these points has been tracked through each of the successive acquired images. According to the authors, the performance of the proposed 3D-DIC UAV proved its accuracy in measuring the evolution of displacements characterizing the expansion and the contraction of the joints with an accuracy comparable with that obtained with a dial caliper. The non-contact aspect of the optical measurement approach also allows for more frequent and cost-effective measurements of bridge conditions.

# 3. Case study

The presence of natural joints in concrete dams might weaken their strength, rigidity and impermeability, endangering the serviceability. The dam considered herein is an arch-gravity dam with a large scale influential horizontal crack on the downstream face. The performed analysis aims to assess the contribution of the crack propagation on the dam displacements. Of particular interest are the variations of crest displacement and crack opening displacement of the dam subjected to thermal loading, owing to a variation in the crack length.

## 3.1 Description of the dam and monitoring system

"Chencun" dam is a concrete arch-gravity dam located on Qinghe River in Huangshan City, China. The dam has a maximum height of 76.3 m and a crest length of 419 m; its crest elevation is 126.3 m. The crest width is 8.0 m and the maximum base width is 53.5 m. It is composed of 28 dam blocks (**Figure 19**) (Hu and Wu [3]).

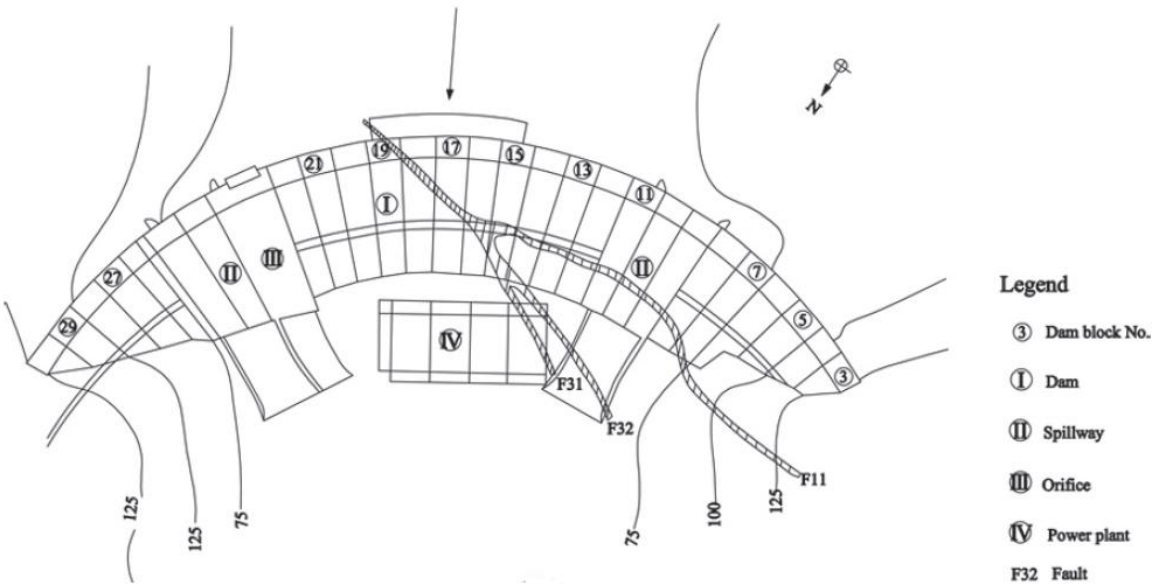


**Figure 19. Layout of the dam**

The dam site is located on a curved bedrock with complex geological U shaped conditions. Its topography is asymmetrical and the left bank is

relatively steeper. Faults developed in the dam foundation, and there are multiple sets of faults cutting each other. The design flood and the dead reservoir levels are EL 124.60, and 101.00 m, respectively. The construction was divided into three phases, namely, 1959–1962, 1969–1972, and 1978, when the dam crest reached EL 105.00, 125.00, and 126.30 m, respectively.
An horizontal crack emerged at the downstream surface at EL 105.00 m near the top of the Phase I section, because the shrinkage deformation of the Phase II section concrete at this location was restrained by the hardened concrete of Phase I. The crack stretches horizontally with 300 m length and more than 5 m depth. Most of the crack mouth opening displacements (CMODs) were in the range of 0.1–0.5 mm, with individual segments reaching a maximum of 7.0 mm. In 1972, an epoxy grouting treatment was carried out for crack segments which were wider than 0.5 mm. In 1987, the crack was re-treated using a modified epoxy resin, which is characterized by small viscosity, fast curing speed, little heat release, and high strength. After grouting, the core samples were drilled and checked, and the results proved that the epoxy reached a depth of more than 1.0 m. However, CMODS had been continually increasing even after reinforcement treatment, accompanied by abnormal deformation characteristics of the dam. The crack development, in the dam in both longitudinal and cross sections, is shown in **Figure 20**.

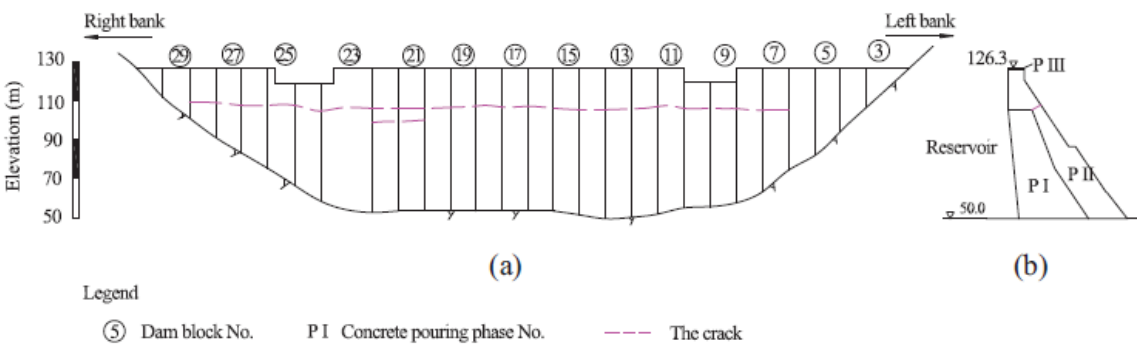


**Figure 20. Crack development in the dam: (a) longitudinal section (downstream) showing crack traces near EL 105.00 m and (b) standard cross-section showing relative locations.**

As of the monitoring system, plumb lines have been in service for more than 40 years. They were mainly arranged in the crown cantilever Block 18 and the left and the right 1/4 arches (i.e. Blocks 8 and 26) to measure horizontal movements of the dam body: radial displacement is positive toward downstream, and tangential displacement is positive toward the right bank. **Figure 21** shows the plumb lines of the different blocks and in **Figure 22** the long time series of radial monitoring data of plumb lines are plotted.

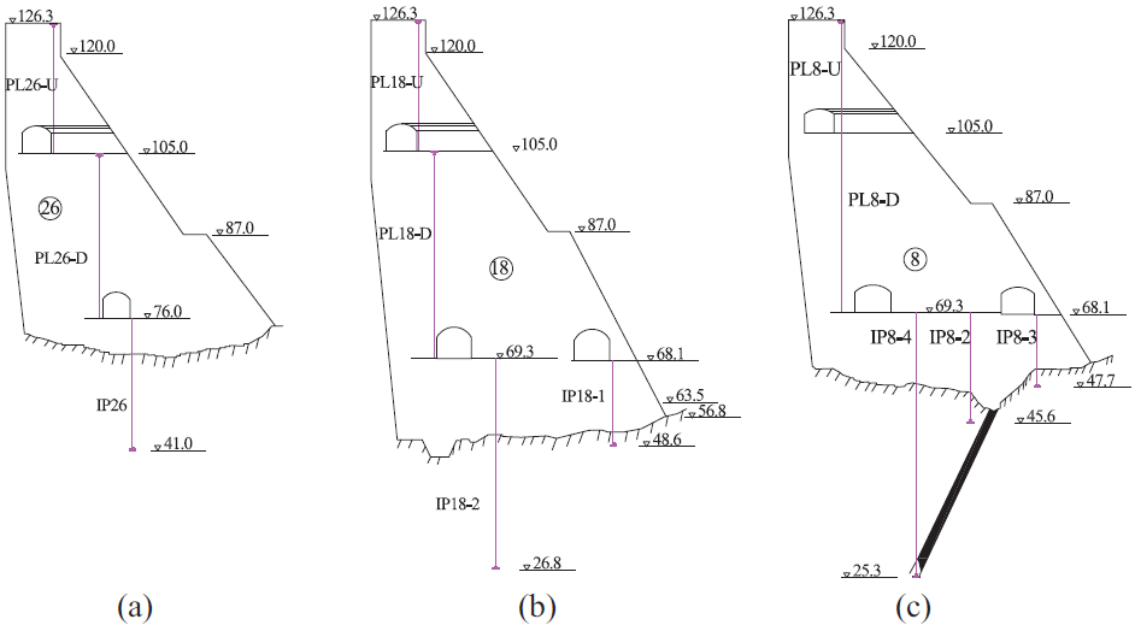


**Figure 21. Locations of plumb lines: (a) Block 26, (b) Block 18, and (c) Block 8; elevations are given in meters.**

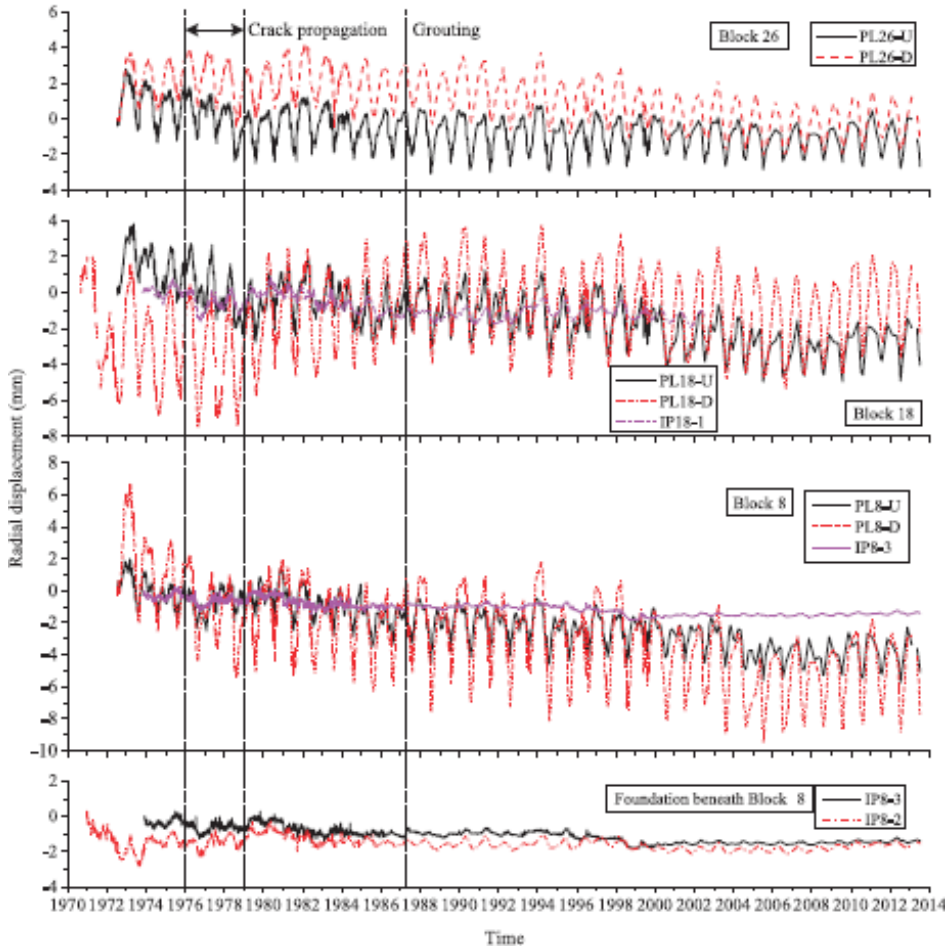


**Figure 22. Measured radial displacements of dam blocks and foundation under Block 8**

Twenty one measuring points were installed to monitor the dynamic change of CMOD. The measurements have been carried out since 1972 and they are currently performed once a week to ensure continuity. The historical time series of a measuring point installed in Block 18 are shown in **Figure 23** .

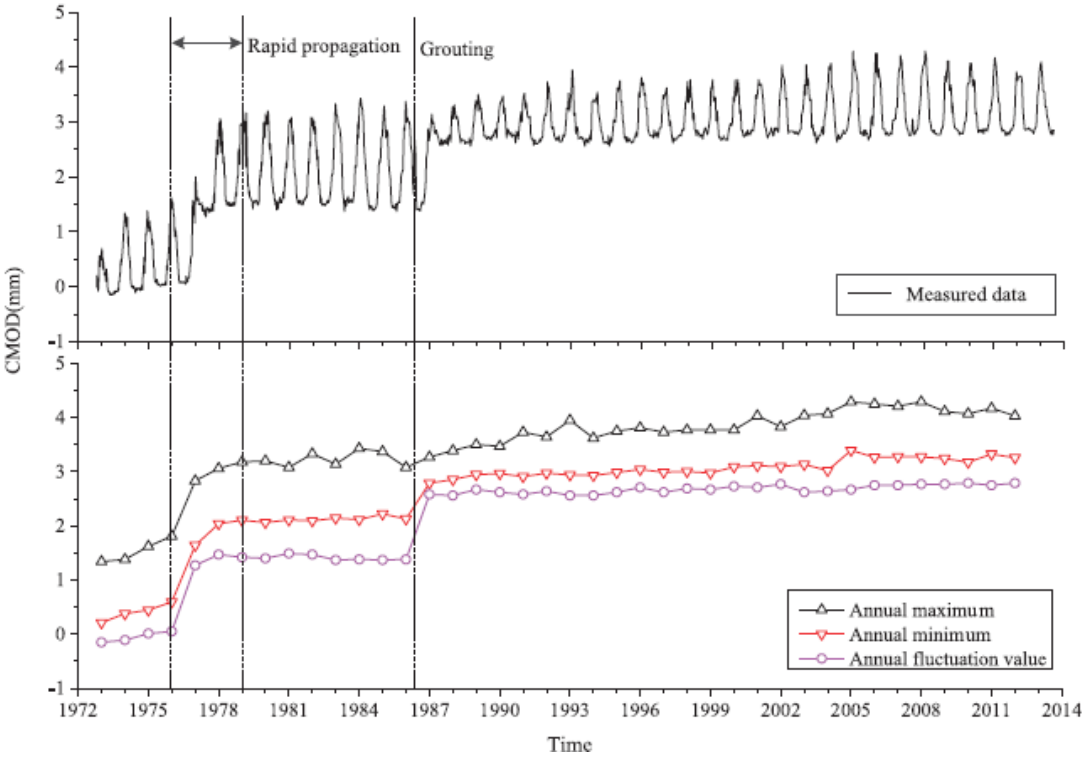


**Figure 23. CMOD and annual fluctuations of the crack segment in Block 18**

The long time series of **Figure 23** shows that, except for the two jumps in the late 1970s and 1987, the CMOD generally presents a regular annual periodicity and a certain trend of growth. From July 1976 to April 1979, the reservoir level for 720 out of 980 days was lower than the dead water level (EL 101 m) and the CMODs experienced a propagation process due to the upstream deformation of the dam crest. In 1980s, the reservoir level rose and the CMOD slowed down from the rapid growth. But in the spring of 1987, the measured CMOD values increased suddenly, which was caused by the modified epoxy grouting. The latter is equivalent to inserting a wedge at the crack tip, restricting the free closure of the crack under high temperature condition and increasing the minimum CMOD. On the other hand, the CMOD is also closely related to air temperatures. Low temperature directly results in the contraction of dam concrete and opening of crack mouth. **Figure 24** presents the historical variations of daily mean reservoir level and daily air temperature.

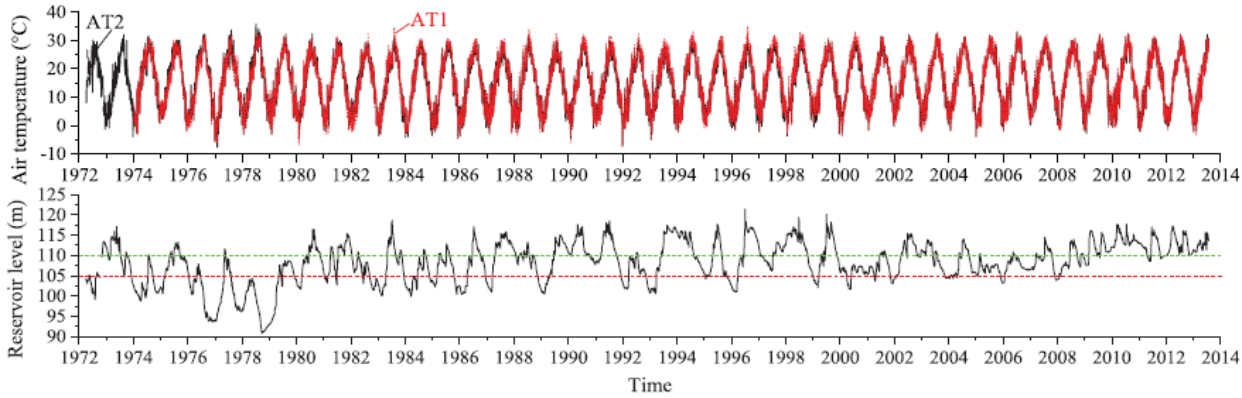


**Figure 24. Variations of mean daily air temperature and reservoir level**

Ultrasonic pulse velocity (UPV) tests were conducted to detect the direction and depth of the crack in 1984 and 2004. In 1984, UPV tests were carried out to detect crack segments in the eight blocks: Blocks 12–15 and 18–21 (Hu and Wu [3]). UPV test is an in-situ, non destructive test that can be used to check the quality of concrete. The testing equipment includes an electronic circuit for generating pulses, a transducer for transforming electronic pulses into mechanical pulses, and a pulse reception circuit that receives the signal. The test is conducted by measuring the time taken by the generated ultrasonic pulse to travel through the material. The higher the velocity, namely the less the travel time, the better the quality and continuity of the material. The pulse velocity for ordinary concrete ranges from 3700 to 4200 m/s. Voids, cracks and aggregate particles in concrete actually scatter a part of the initial energy of the wave pulse away from the original wave path. Ultrasonic pulses are characterised by frequencies greater than 20 kHz. The path length that can be effectively taken into account at the frequency of 20 kHz, before having a complete scattering, is of several meters. The lower the frequency, the higher the path length that can be investigated. Depending on the positioning of the two transducers (transmitter and receiver), the type of reading can be: direct, semi direct or indirect (**Figure 25**).

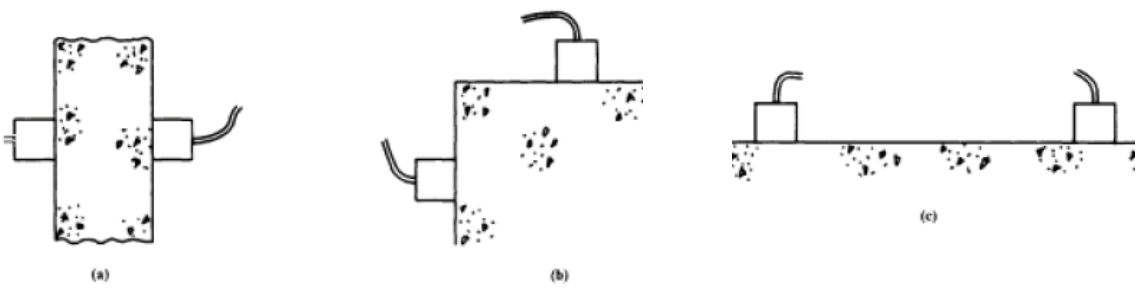


**Figure 25. Type of reading: (a) direct, ( b) semi-direct, (c) indirect**

UPV tests can be effectively used for detecting cracks through the use of indirect surface readings. A pair of 40-kHz narrowband transducers with a diameter of 30 mm was used for the measurements. Core tests were also carried out to verify the results of UP tests. The results of the two tests were consistent. In 2004, crack segments in the eight blocks 7, 12–14, and 18–21 were examined by UP tests. The results show that the crack depths of Blocks 7, 12, 13, and 21 were in the range of 5.3–5.7 m and the crack depths of Blocks 14, 18, 19, and 20 were 4.2, 2.7, 3.9, and 3.7 m, respectively. The width of the Phase II section at EL 105.00 m is about 6.0 m. From UP test results, the crack had already passed through the Phase II section and terminated at the joint between the Phase I and II sections, due to the limitation of this structural joint.

## 3.2 Finite Element analysis

The simplified approach proposed by Colombo and Domeneschi [26] has been followed in order to perform a 2D finite element (FE) analysis investigating the effects of the crack propagation on the Chencun dam Block 18 deformation behaviour. The latter approach decouples the thermal from the mechanical regime, executing in sequence first a transient thermal analysis and a linear elastic static analysis. In particular, Abaqus software has been used in order to carry out the 2D finite element analyses of the dam-foundation system representing Block 18, which is characterised by the tallest cross section. The use of two dimensional analyses in dams are a common practice since, in most cases, they yield sufficiently accurate results and for practical purposes (Tanchev [2]). Factors influencing the choice between two and three dimensional analyses are the shape of the canyon and the degree of constraint that the transverse contraction joints impose to the adjacent monoliths. Two dimensional analyses are more suitable for dams situated in U shape canyons than narrow canyons. Moreover, 2D analyses better suite dams whose monoliths behave separately rather than dams behaving as a monolithic solids (De Falco et al. [27]). Information on the degree of restraint of a monolith due to the adjacent ones might be provided by the monitoring of opening displacements of transverse contraction joints.

Different FE meshes have been chosen for thermal and mechanical analyses. In particular for the transient thermal analysis of the dam body, a rougher mesh has been adopted (**Figure 26**).

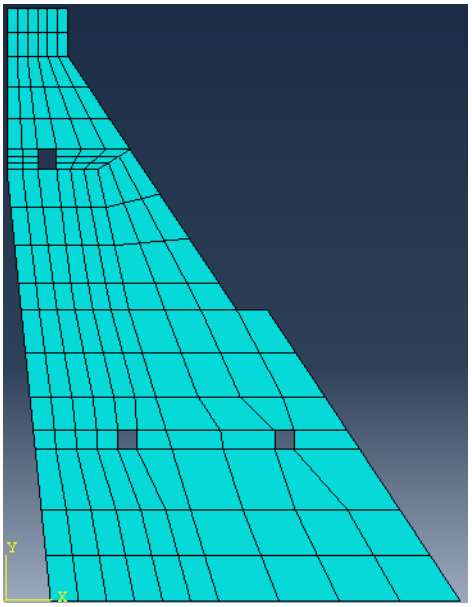

**Figure 26. Rougher mesh adopted for the thermal analysis**

As of the linear elastic static analysis, two FE models have been built, considering 4 and 5 meter long crack, respectively. The second model represents the situation in which the crack has propagated until the joint between the Phase I and Phase II. The cracks have been modelled as unsealed, namely the epoxy grouting treatments have not been considered. For both configurations, the dam inspection galleries, as well as the rock foundation have been modelled. The meshes adopted for the dam body in the first and second configurations are shown in **Figure 27** and **Figure 28**, respectively.

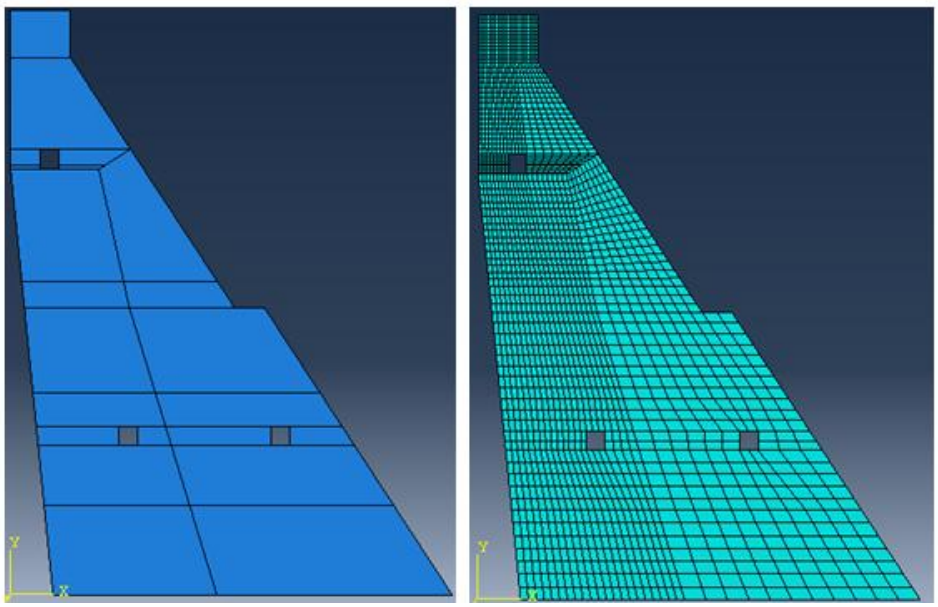

**Figure 27. First FE model (4 meter long crack) adopted for the mechanical analysis**

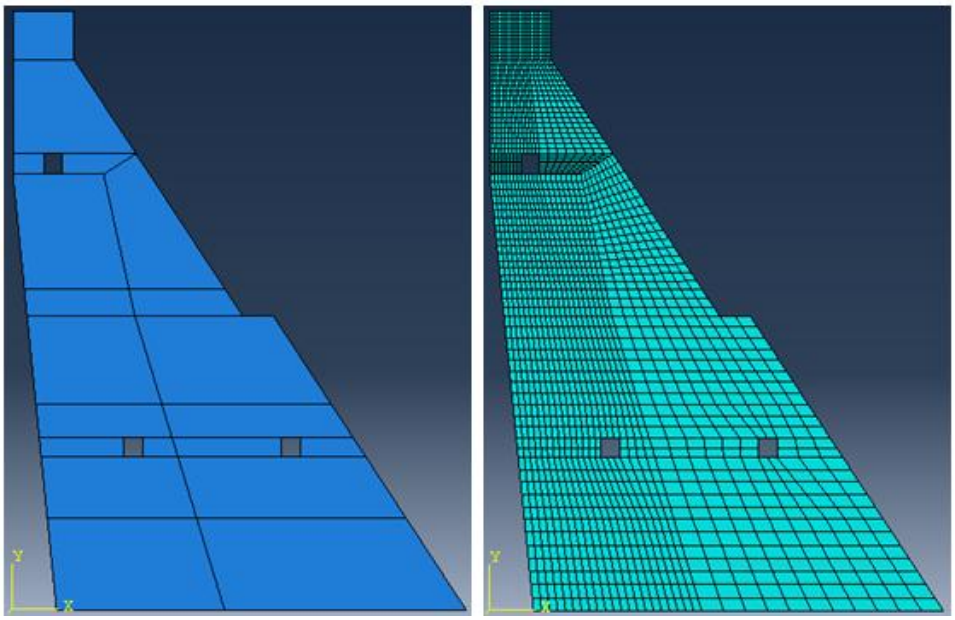

**Figure 28. Second FE model (5 meter long crack) adopted for the mechanical analysis**

In **Figure 29**, both the dam body and its rock foundation, for the first model (4 meter long crack), are shown.

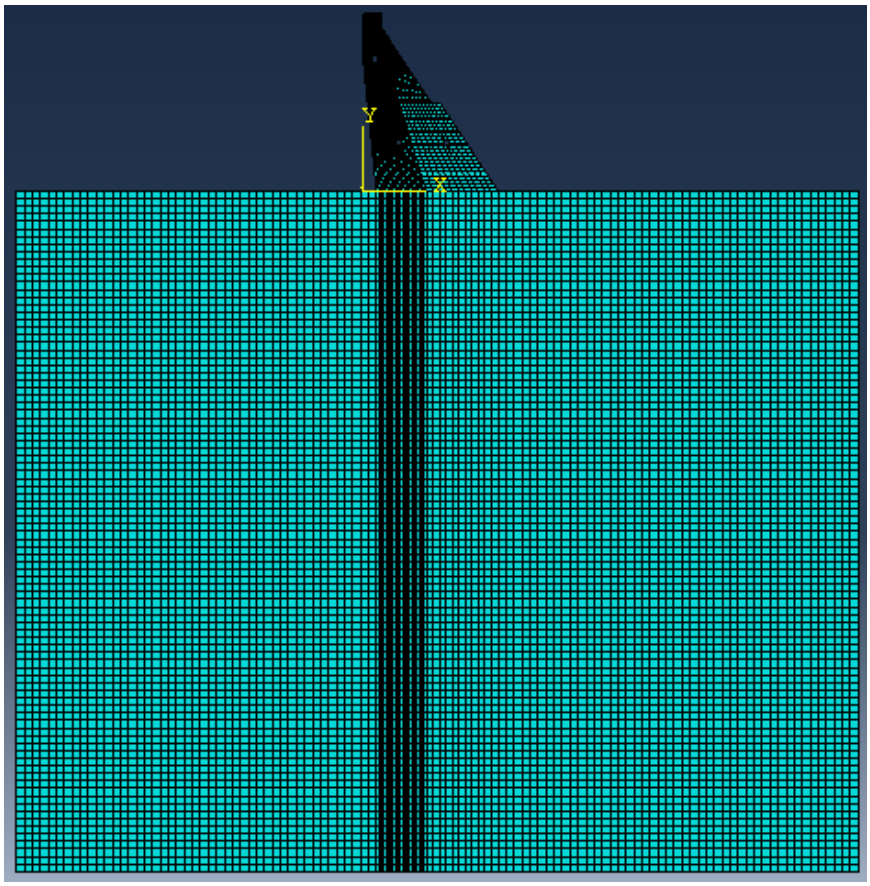

**Figure 29. Mesh of the dam body and its rock foundation for the first FE model (4 meter long crack)**

Regarding the thermal analysis, heat transmission into the dam body is typically conductive and can be modelled imposing thermal boundary conditions at the mesh nodes belonging to the dam external surface. Heat transmission by conduction is governed by the Fourier's law. The latter states that the rate of heat transfer between two surfaces with solid material between them is proportional to the area of the surfaces and the temperature difference between them, while it is inversely proportional to the distance between them:

$$\rho C \frac{\partial T}{\partial t} = \mathrm{div}\left(\vec{k}\,\mathrm{grad}T\right) + Q$$

where,

ρ is the density of the material [kg/m$^3$];

C is the specific heat [J/kg°C];

k is the thermal conductivity [W/m °C];

Q is the internal heat generated for a unit volume in a unit time [W/m$^3$];

The density of concrete has been set equal to 2400 kg/m$^3$. As far as thermal properties of the dam concrete are concerned, specific heat equal to 900 J/kg°C and thermal conductivity equal to 2 W/m °C have been considered.

As of the thermal boundary conditions, a zero heat flux condition has been applied at the boundaries of the foundation, while air and water temperatures have been applied on the other boundaries of the model. Thermal boundary conditions in terms of air temperature have been imposed at the mesh nodes according to the regression equations of thermometers of air temperature at the dam site. The latter equations have been obtained using the least square method, based on temperatures measured by thermometers (Hu and Wu [3]). The equations at two different locations (AT1 and AT2) are:

$$T_{AT1} = 15.78 - 4.84 * \sin\left(\frac{2 * \pi * t}{365}\right) - 11.20 * \cos\left(\frac{2 * \pi * t}{365}\right)$$

$$T_{AT2} = 15.50 - 4.59 * \sin\left(\frac{2 * \pi * t}{365}\right) - 10.88 * \cos\left(\frac{2 * \pi * t}{365}\right)$$

where t represents the number of days from the first day of the year until the observation date. The interpolation of the two thermometers of air temperature was used as the boundary temperature of the downstream dam surface between elevation 86.5 and 105.0 m. It is worth observing that thermal boundary conditions can be considered cyclically repeated every year, because of the hydropower service of the structure. The two locations AT1 and AT2 are shown in **Figure 30.**

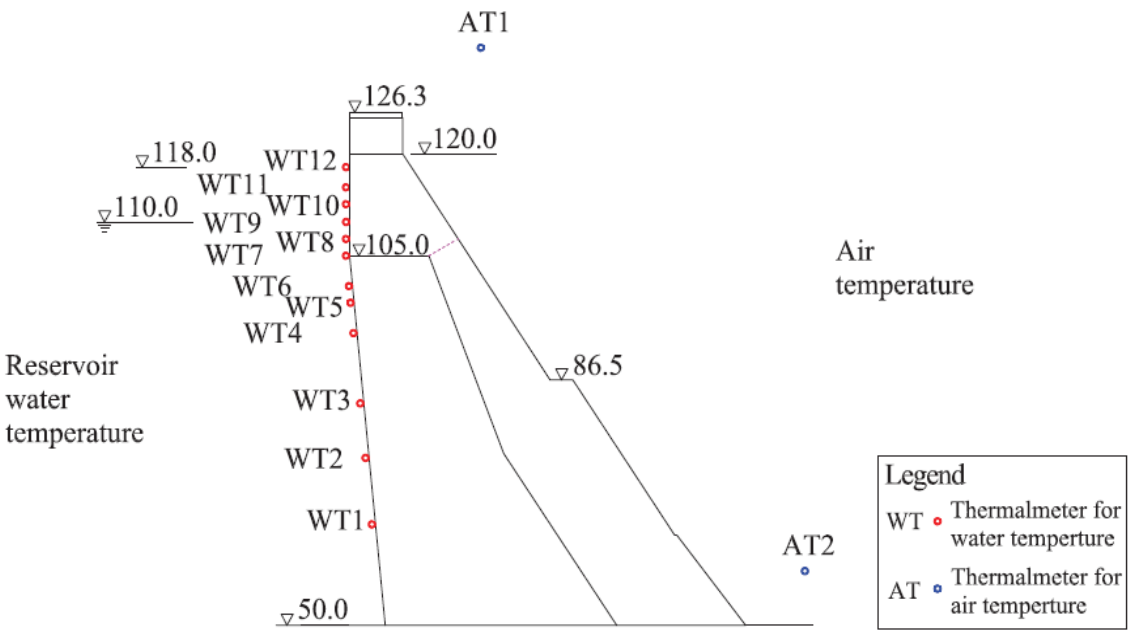


**Figure 30. Location of thermal boundary conditions; elevations are given in meters**

Air temperatures in the three inspection galleries of the dam have not been recorded. However, the galleries are supposed to be long and airtight, therefore air temperature is set as a constant equal to the mean annual temperature of the dam site (Li et al. [28]).

**Figure 30** also shows the locations where the water temperatures have been measured. The time history of the daily water temperature is plotted in **Figure 31** for the different locations.

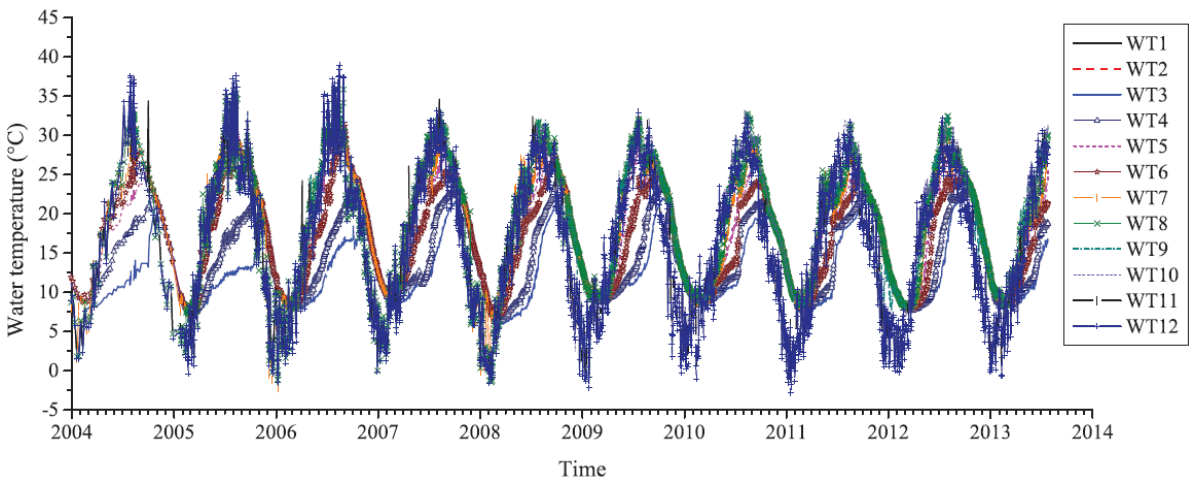


**Figure 31. Water temperatures at different depths of the reservoir from 2004 to 2014**

The time histories of daily water temperatures (**Figure 31**) and the location of the measurement points (**Figure 30**) have not been considered in order to determine the boundary conditions in terms of water temperature. This is owing to the fact that both data were only available in the form of a graphical representation, whose numerical quantification is arduous.

Alternately, the variant of the Bofang's formula [29] by Sheibany and Ghaemian [30] has been used, with some additional modifications. The water temperature T at depth y and time t for the reservoir of the Chencun dam becomes as follows:

$$T(y,t) = T_m(y) + A(y)\cos[\omega(t - t_0 - \xi)] \qquad T \geq 4°C$$

with:

$$T_m(y) = C + (18.2 - C)\, e^{-0.04\, y}$$

$$C = \frac{6 - 18.2\, g}{1 - g}$$

$$g = e^{-0.04\, H}$$

$$A(y) = 11.8\, e^{-0.018\, y}$$

$$\xi = 54 - 39.42\, e^{-0.085\, y}$$

$$\omega = \frac{2 * \pi}{365}$$

where:

y is the depth of the water $[m]$;

t is the time $[day]$;

$T(y,t)$ is the temperature at depth y and time t $[°C]$;

$t_0$ $[day]$ is the time at which air temperature is maximum (210 days);

H is the reservoir water depth $[m]$.

The reservoir water depths have been considered according to the following periodic approximation function:

$$H = 60 - 8 * \cos\left(\frac{2 * \pi * t}{365} - 0.55\right),$$

and reported in **Figure 32.**

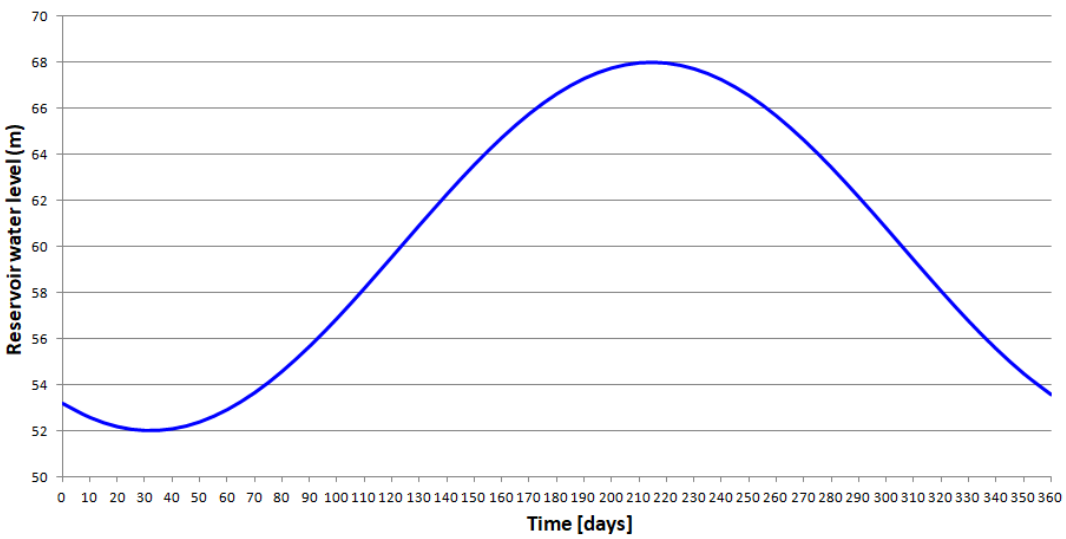


**Figure 32. Approximated reservoir water depths**

The air temperatures $T_{AT1}$and $T_{AT2}$ are shown in **Figure 33**.

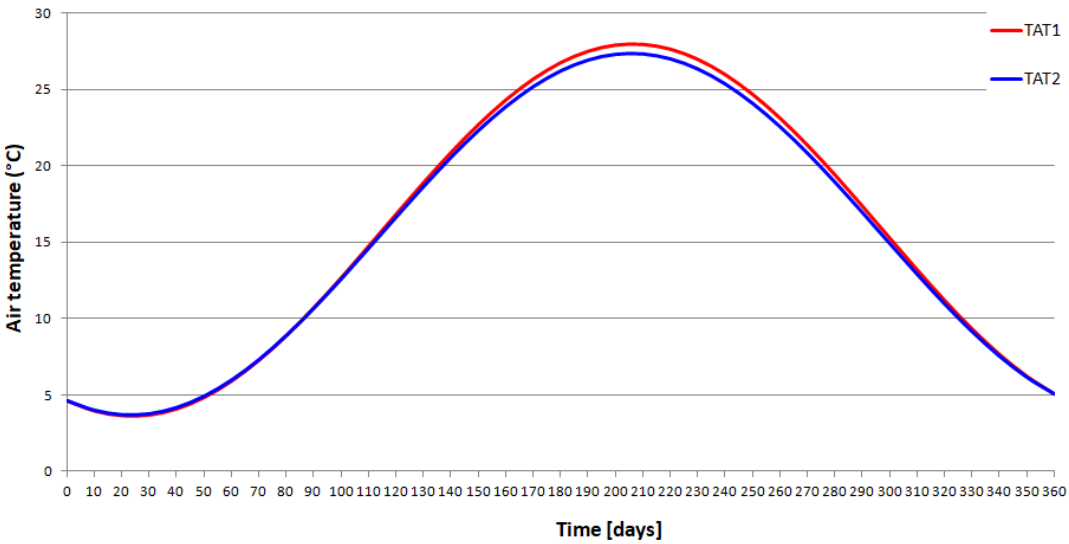


**Figure 33. Daily mean air temperature variations at locations AT1 and AT2**

In **Figure 34,** the mean value TA of the air temperatures $T_{AT1}$and $T_{AT2}$ is plotted together with the computed temperatures at different depths $T(y,t)$.

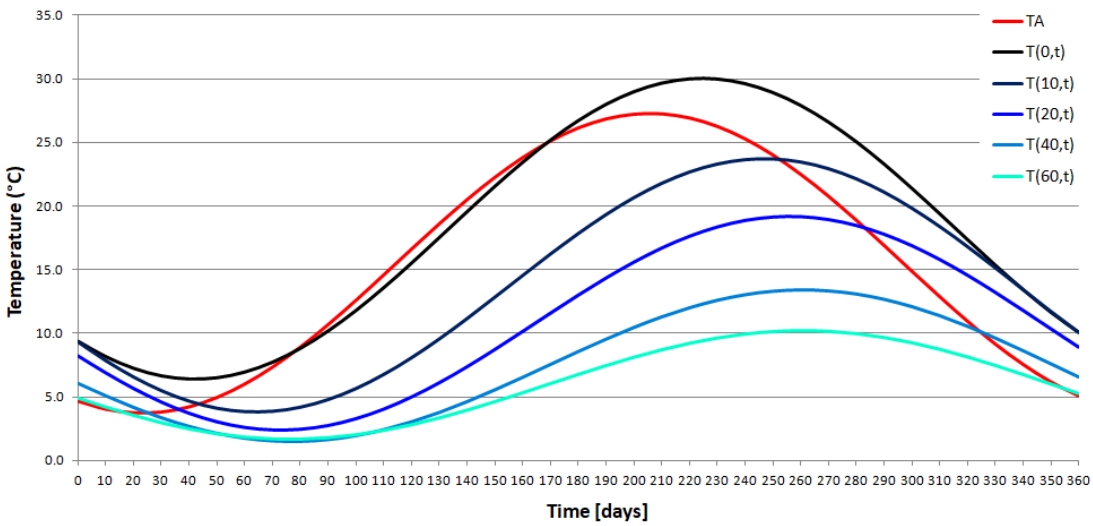


**Figure 34. Comparison between the mean of the air temperatures $T_{AT1}$and $T_{AT2}$ and the computed temperatures at different depths**

When applying thermal boundary conditions, thermal convection coefficients must be set. The thermal flux between the fluid and the surface by means of convection is expressed as:

$$q = \alpha_c A \left(t_{surface} - t_{fluid}\right)$$

where:

q is the thermal flux $[W]$;

$t_{surface}$ and $t_{fluid}$are the temperatures of surface and fluid respectively $[°C]$;

A is the area of the surfaces $[m^2]$;
$\alpha_c$ is the thermal convection coefficient $[W/m^2°C]$;

Convection coefficients have been set equal to 13 $W/m^2°C$ for air and to 500 $W/m^2°C$ for the reservoir water. Exploiting thermal boundary conditions, the thermal analysis has been carried out and temperature fields within the dam have been obtained. Heat transfer calculations have been carried out with time steps equal to 10 days, imposing, at the mesh nodes, time varying thermal boundary conditions and convection coefficients. For instance, some nodes belonging to the upstream face of the dam are in contact with either water or air due to the fluctuation of the reservoir water level during the year. For those nodes, the thermal boundary conditions are varying in time in terms of both temperature and convection coefficient. On the other hand, the nodes that are either underneath or above the reservoir water level for the whole duration of the analysis are characterised by time varying temperatures and constant convection coefficients.

As concrete temperature at time zero, the joint closure temperature at different elevations and for both Phase I and Phase II has been considered. (**Table 1**) (Hu and Wu [3]).

| Elevation (m) | Closure temperature (°C) | |
|---|---|---|
| | Phase I section | Phase II section |
| 111.20 - 105.00 | - | 16 |
| 105.00 - 90.00 | 13 | 16 |
| 90.00 -75.00 | 11 | 15 |
| 75.00 - 60.00 | 10 | 14 |
| 60.00 - 48.00 | 9 | 13 |

**Table 1. Closure temperatures at different elevations of the dam**

The heat transfer calculations have been carried out for additional 365 days in order to obtain more regular temperature distributions.

The linear elastic static mechanical analysis of Block 18 has been performed in plane strain conditions. As of mechanical properties of concrete, elastic modulus equal to 19 GPa, Poisson's ratio equal to 0.167 and density equal to 2400 $kg/m^3$ have been set. (Hu and Wu [3]). Regarding the loading conditions, dam self weight, hydrostatic loads and point-wise thermal loads have been considered. Shrinkage and heating phenomena generated by concrete hydration are considered completed, since the considered dam has a service life of decades. Therefore, residual stresses due to the concrete viscosity have been disregarded. Moreover, in the considered dam, effects arising from alkali silica reactions have not been significantly detected, consequently they have not been considered.

The dam self weight is computed as:

$$G = \sum V \Upsilon$$

where:
V is the volume of the dam $[m^3]$
$\Upsilon$ is the unit weight of concrete $[kg/m^3]$
The unit weight of concrete is computed as the product of gravitational acceleration and concrete density. It is worth pointing out that the dam self weight is not considered in the analyses for which a comparison between computed displacements and displacements measured by pendulums is foreseen. In those cases, the effects exerted by the dam self weight are already included at the installation of the instruments.
Hydrostatic loads are composed by hydrostatic and uplift pressures owing to the dam reservoir. The hydrostatic pressure, at the depth $h_i$, acting on the dam upstream face of the dam is computed as:

$$p_i = \rho \, g \, h_i$$

where:
$p_i$ is the hydro-static pressure at water depth $h_i$ $[Pa]$
$\rho$ is the density of water $[kg/m^3]$
g is the gravitational acceleration $[m/s^2]$
$h_i$ is the specific water depth $[m]$

The uplift pressure is considered as a triangular pressure acting on the bottom surface of the dam, that has its maximum value in correspondence of the upstream edge and a value equal to zero in correspondence of the downstream edge. The maximum value has been considered equal to the value of the hydrostatic pressure at the bottom.
As of thermal loads, the temperature distributions obtained from the thermal analysis have been used as input for the structural deformation model. At each mesh node, the thermal strains induced within the dam body due to the temperature variations are imposed as:

$$\varepsilon_{ij}^{term}(x,t) = \alpha \, \Delta T(x,t) \delta_{ij}$$

where:
$\varepsilon_{ij}^{term}$ is the thermal strain $[-]$
$\alpha$ is the thermal expansion coefficient $[°C^{-1}]$
$\Delta T(x,t)$ the temperature variation $[°C]$
$\delta_{ij}$ is the Kronecker's delta $[-]$

Thermal expansion coefficient equal to $10^{-5}\,°C^{-1}$ has been set. The temperature variation $\Delta T(x,t)$ is the difference between the thermal analysis results at each node of the mesh at the day of the analysis and the nodal joint closure temperatures.
As far as the foundation of the dam is concerned, the size of the rock foundation to be included has been set such that its boundaries were characterised by a value of von "Mises equivalent stress" equal to zero. The elasticity modulus and Poisson's ratio of the rock foundation has been considered to be equal to 19 GPa and 0.2, respectively.
The crack has been modelled creating two different parts for the dam body, whose nodes, at the elevation of the crack, are characterised by the same coordinates. Then, a "tie" interaction has been used for the nodes not characterised by the crack and a "surface to surface contact" with hard' and "frictionless" contact has been used for the crack modelling.

## 3.3 Results of the Finite Element analysis

In the following, the results of the thermal analysis are reported. As previously mentioned, the heat transfer calculations have been carried out for additional 365 days in order to obtain more regular temperature distributions. As an example, the temperature distributions of January 20$^{TH}$ are shown for first (left) and second (right) year of computations (**Figure 35**).

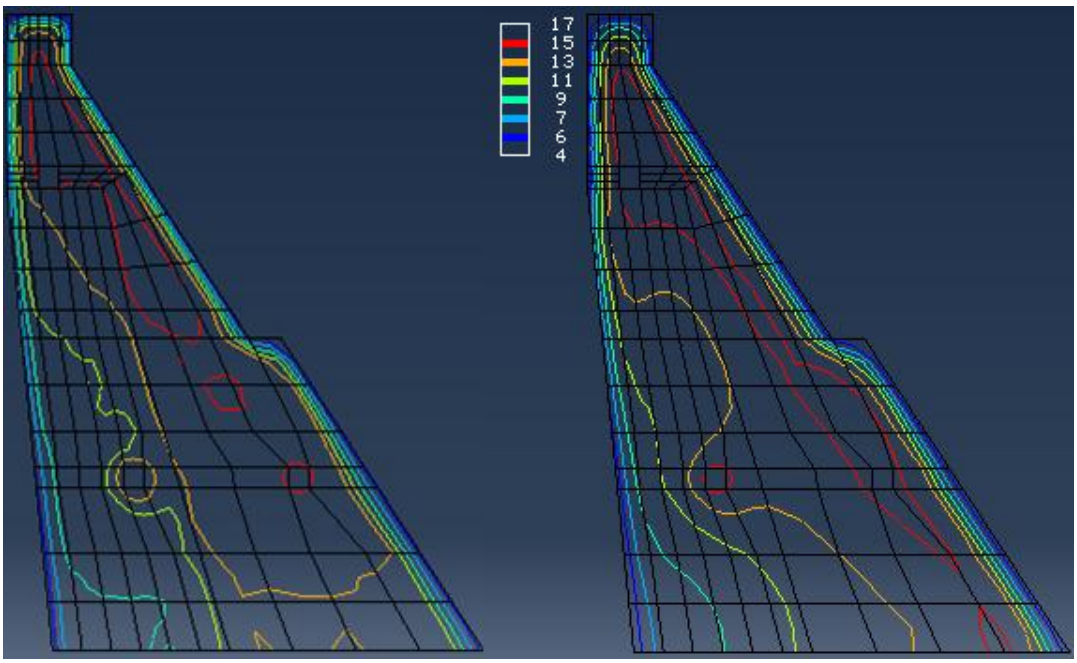


**Figure 35. Temperature distributions (in °C) in Block 18 of January 20$^{TH}$ for the first (left) and the second (right) year of computations**

**Figure 36** shows the annual temperature distribution of Block 18 for the second year of computations.

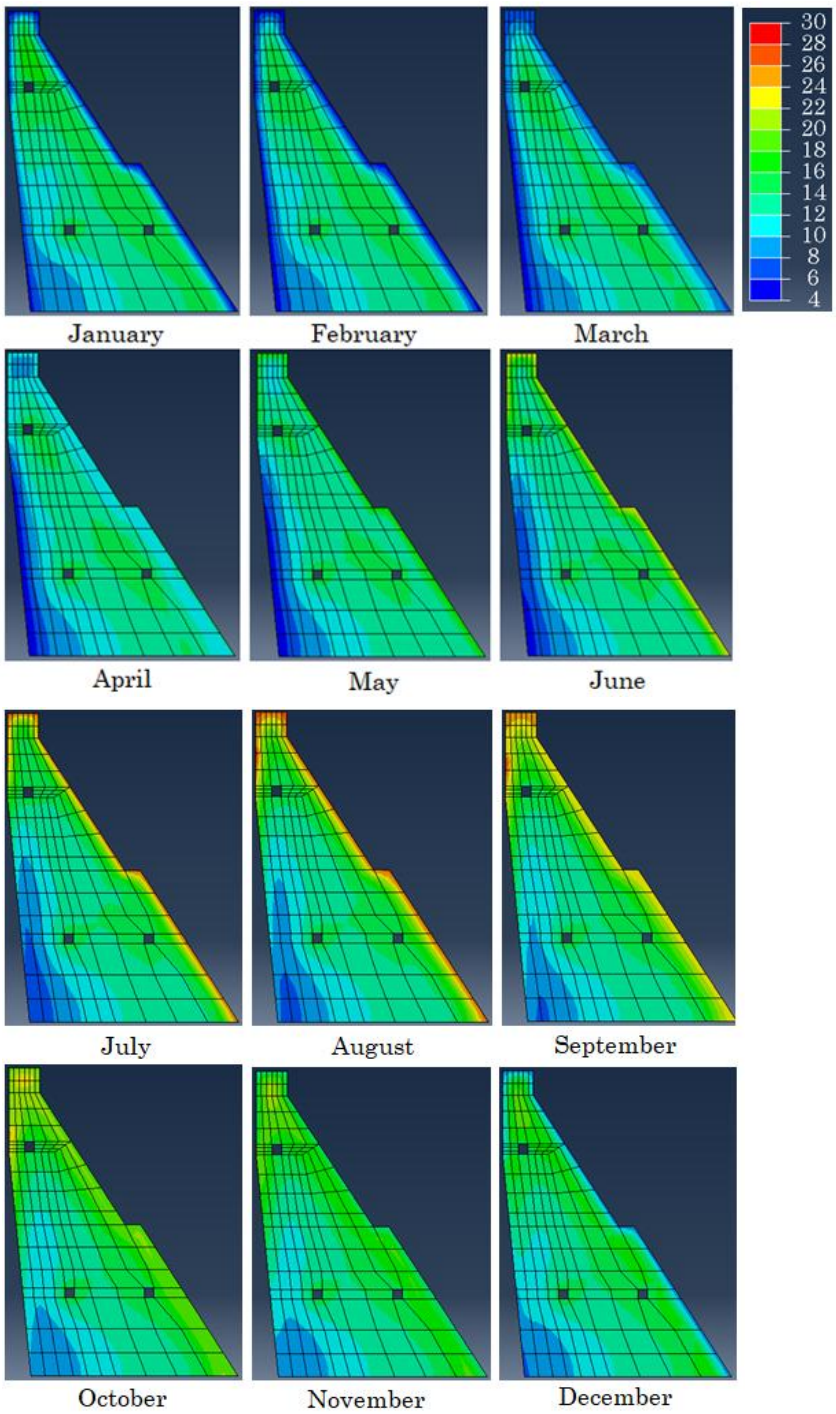


**Figure 36. Annual temperature distribution (in °C)of Block 18 for the second year of analysis**

**Figure 36** shows that water temperature is more effective than air temperature in the temperature distribution of the dam across the thickness.

In the following, the two most critical temperature distributions of the second year of computations are shown: early February (**Figure 37**) and early August (**Figure 38**).

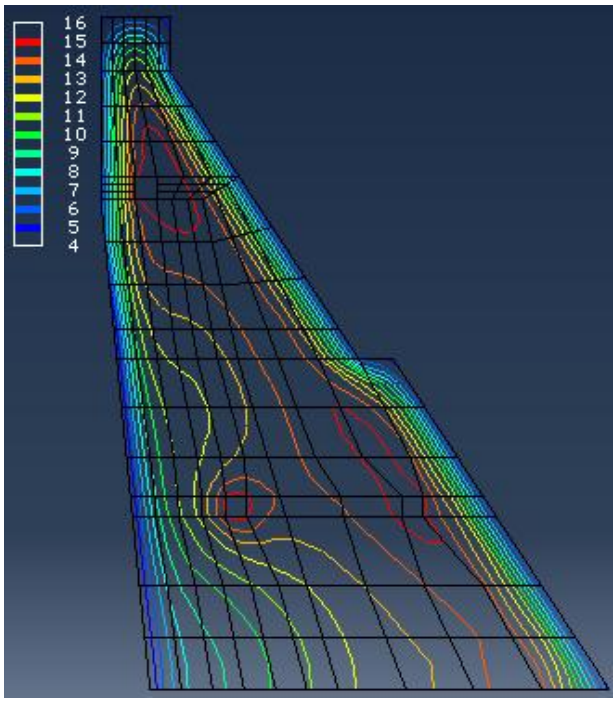


**Figure 37. Temperature distributions (in °C) in Block 18 in early February for the second year of computations**

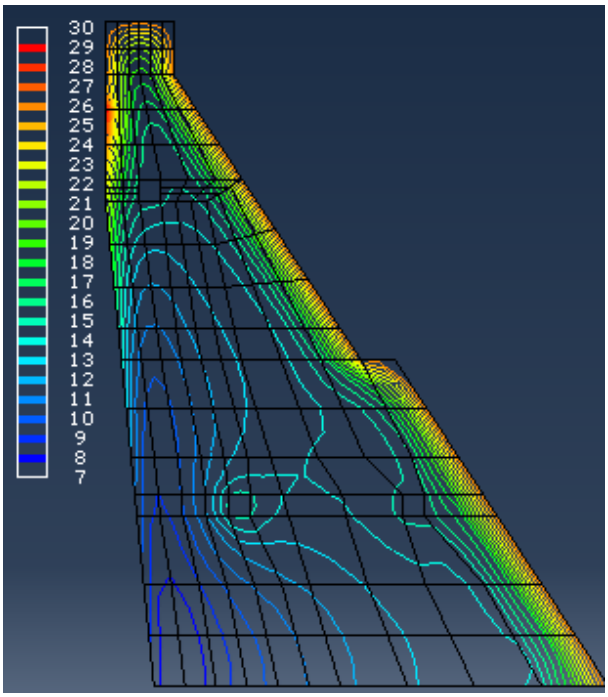


**Figure 38. Temperature distributions (in °C) in Block 18 in early August for the second year of computations**

As of the results of the mechanical analysis, the dam-foundation system of Block 18 with a 4 meter long crack has been analysed under the checked flood level (EL 124.6 m). The resulting upstream- downstream (UP) crest displacement of the model is 12.24 mm.

Subsequently, the aim of the analysis has been investigating the variations of crest displacement and crack opening displacement of the dam subjected to thermal load, owing to a variation in the crack length.

The UD crest displacements of Block 18, under thermal load only, have been computed for both the models (4 and 5 meter long crack) and plotted in **Figure 39.**

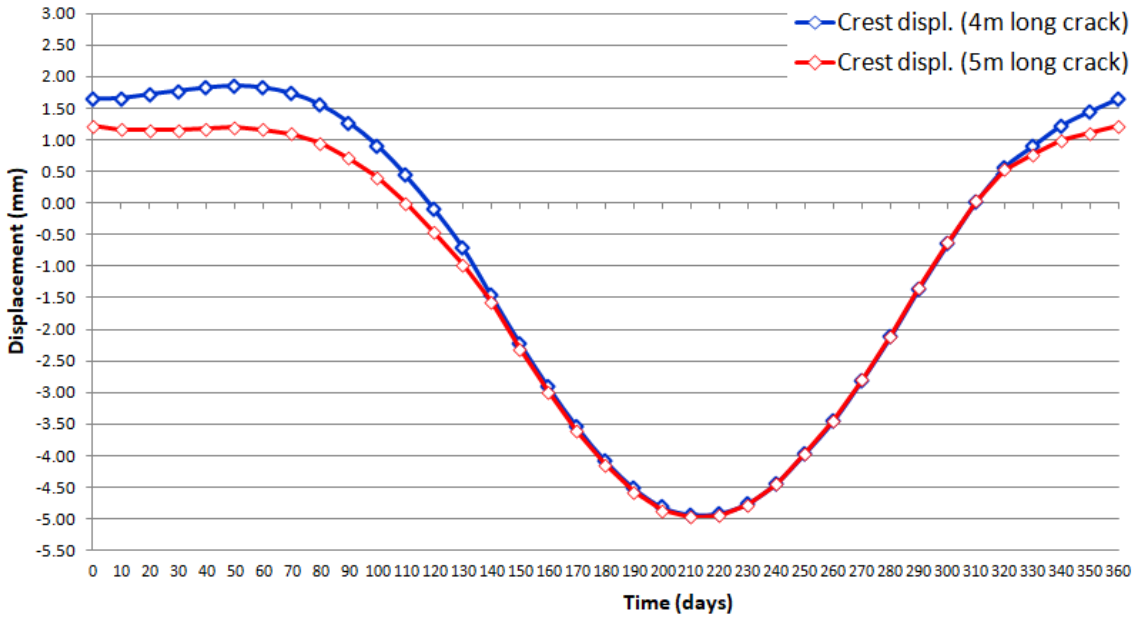


**Figure 39. U-D crest displacements variation of Block 18 after crack propagation**

From **Figure 39** it is possible to observe that the crest UD displacement varies regularly under temperature fluctuation. For the sake of comparison the mean air annual temperature variation is shown in **Figure 40**.

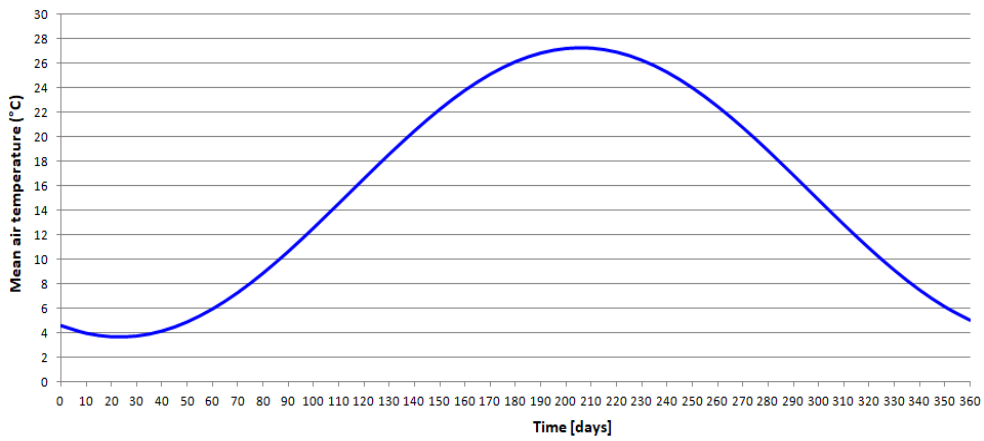


**Figure 40. Mean air annual temperature variation**

From the comparison of **Figure 39** and **Figure 40** , it is possible to notice that during the months characterised by higher temperatures, the dam deforms upstream; while during the months characterised by lower temperatures, the dam deforms downstream. Moreover, during the months characterised by lower temperatures, the crest displacement amplitudes with a 4 meter long crack are larger than those with a 5 meter long crack. The propagation of the crack leads therefore to an amplitude decrease of UD crest displacements. In particular, the maximum U-D crest displacement variation due to crack propagation is observed in early February and its absolute value is 0.66 mm. The differences between the deflection curves of Block 18 of early February and early August under thermal load only, have been computed for both models (4 and 5 meter long crack) and plotted in **Figure 41**, together with the mesh of the first model (4 meter long crack), for visualisation purpose.

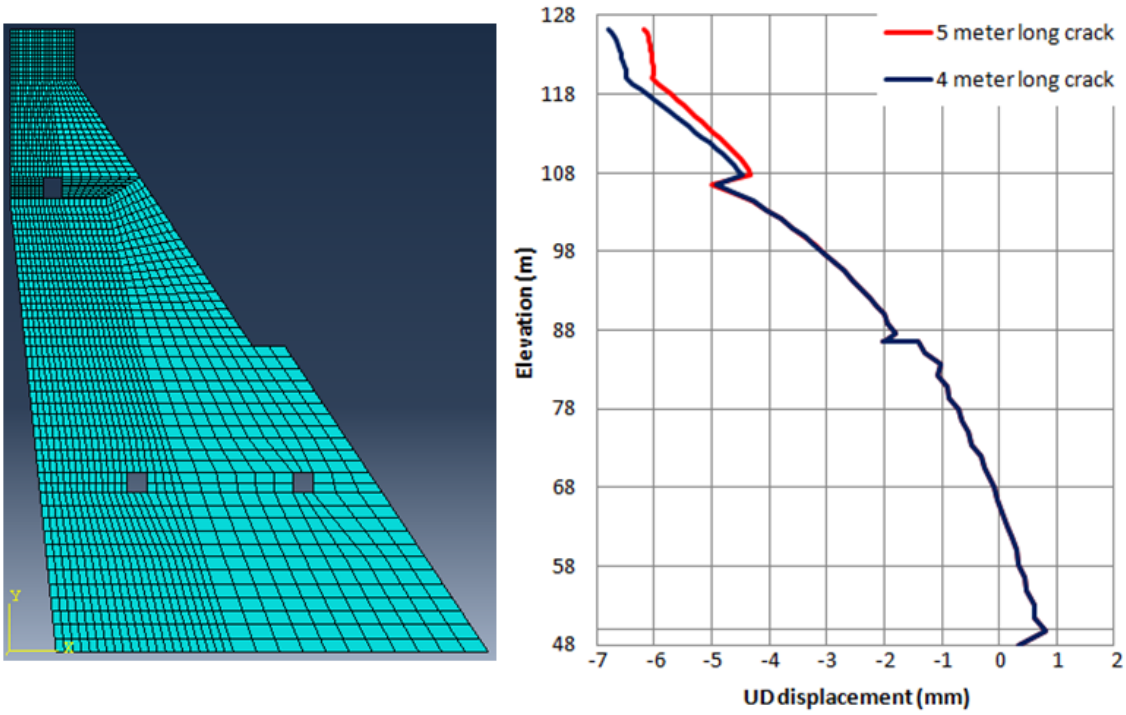


**Figure 41. Computed annual variations of the deflection curve of Block 18 for the two models (4 and 5 meter long crack)**

From **Figure 41** one can observe that the annual variations of the deflection curves are regularly varying with the height of the dam, with the exception of three main locations. Those locations are: the dam base; EL 86.5 m and EL 105 m, which are both characterised by geometrical variations: rock foundation interface, geometry change in the downstream face and inspection gallery and crack, respectively. The two lower inspection galleries do not seem to particularly influence the deflection curves. This might be

due to the fact that at this elevation the dam body is thick and massive. Moreover, **Figure 41** shows that the crack propagation leads to an amplitude decrease of UD displacements for the upper part of the dam only, while, for elevations lower than the elevation of the crack, the annual variations of the deflection curves are almost equivalent before and after the crack further propagation.

**Figure 42** shows the maximum in-plane principal stresses of the upper part of the Block 18 under thermal load only and presenting a 4 meter long crack.

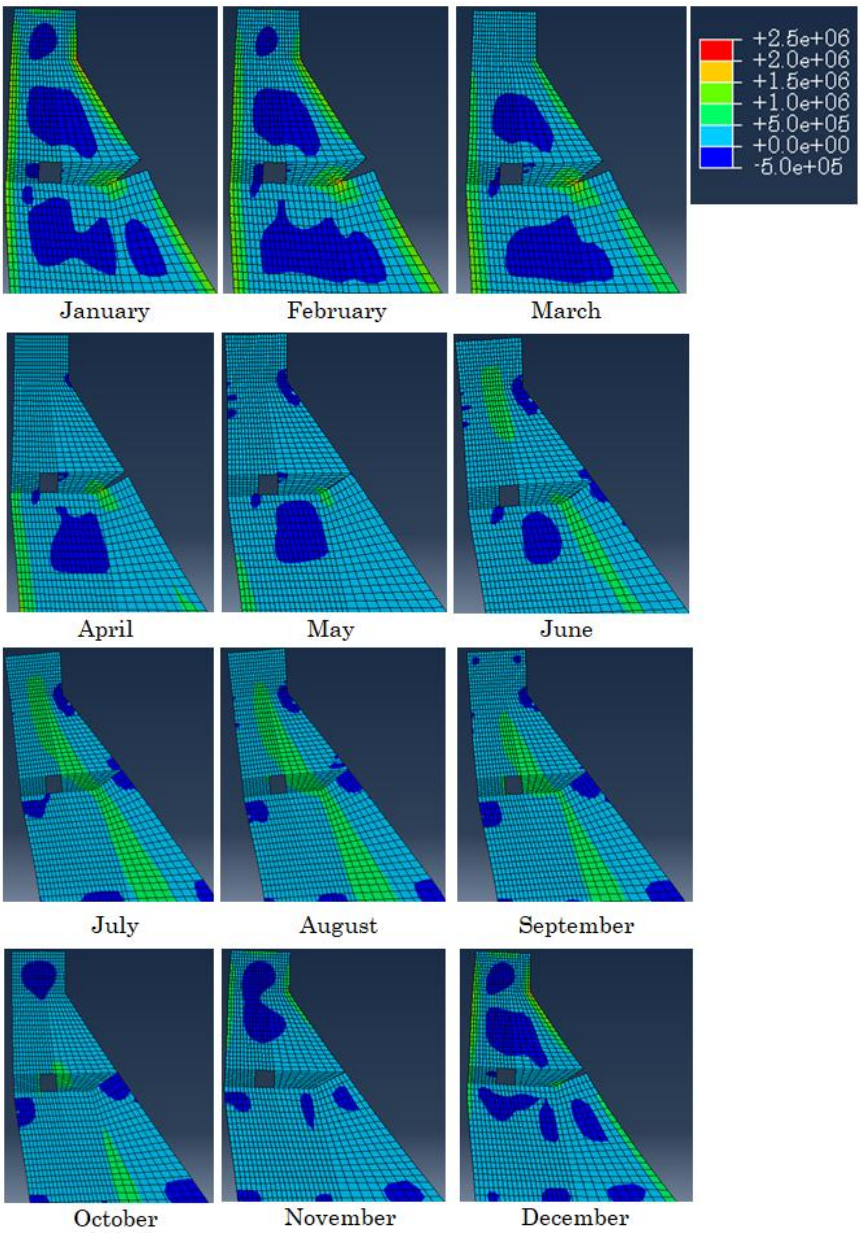


**Figure 42. Maximum in-plane principal stress distribution (in Pa) of the upper part of the dam under thermal load only (4 meter long crack)**

From **Figure 42**, it is possible to observe the opening and closing of the crack in the different months of the year. In particular, one can observe that during the months characterised by higher temperatures (from May to October), the crack closes, while during the months characterised by lower temperatures (from November to April), the crack opens.
In **Figure 43** the two nodes belonging to the two different sides of the crack and located at the downstream face of the dam, are circled.

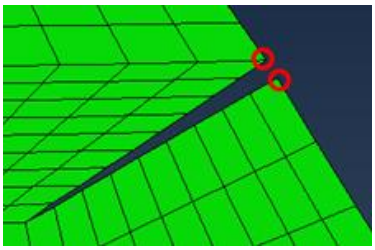

**Figure 43. Nodes belonging to the two different sides of the crack and located at the downstream face of the dam**

The variations of vertical and UD displacements of the two aforementioned nodes have been computed for each step of the analysis of Block 18, under thermal load only, for both the models (4 and 5 meter long crack). Subsequently, the displacements variations have been projected in the directions parallel and perpendicular to the downstream face of the dam. The computed crack opening displacements in parallel to the dam surface are shown in **Figure 44.**

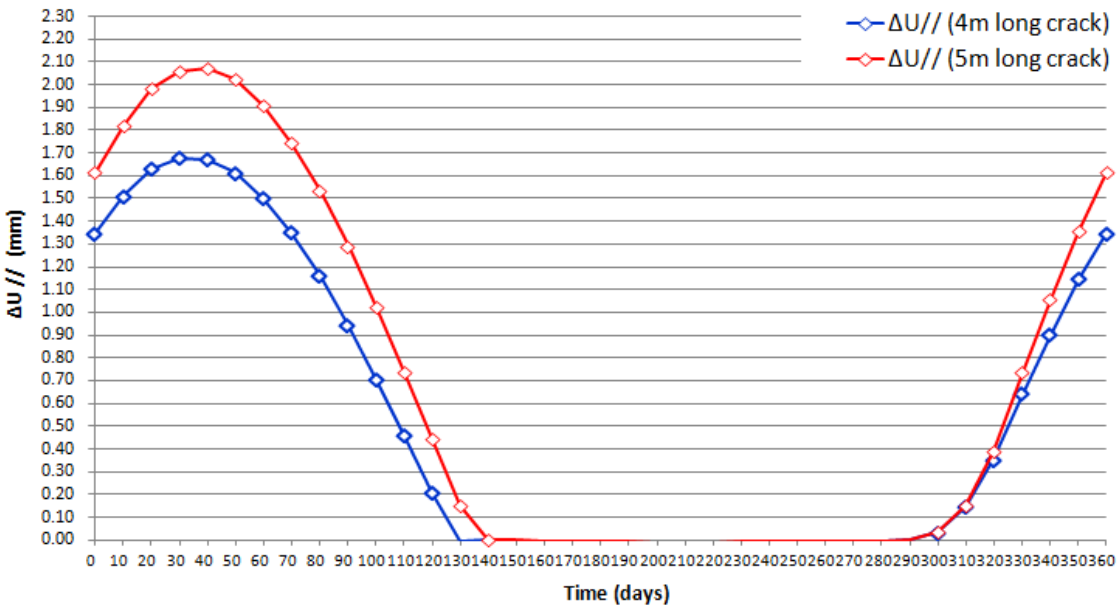


**Figure 44. Computed crack opening displacements in parallel to the downstream surface of the dam**

From **Figure 44** it is possible to observe once again that the crack opens during the months characterised by lower temperatures, while it closes during the months characterised by higher temperatures. Moreover, the 5 meter long crack has higher opening displacements than the 4 meter long crack. The propagation of the crack leads therefore to an amplitude increase of crack opening displacements in the direction parallel to the downstream face of the dam. The latter increase is maximum in early February and its value is 0.41 mm.

**Figure 45** shows the computed crack opening displacements perpendicularly to the dam downstream surface.

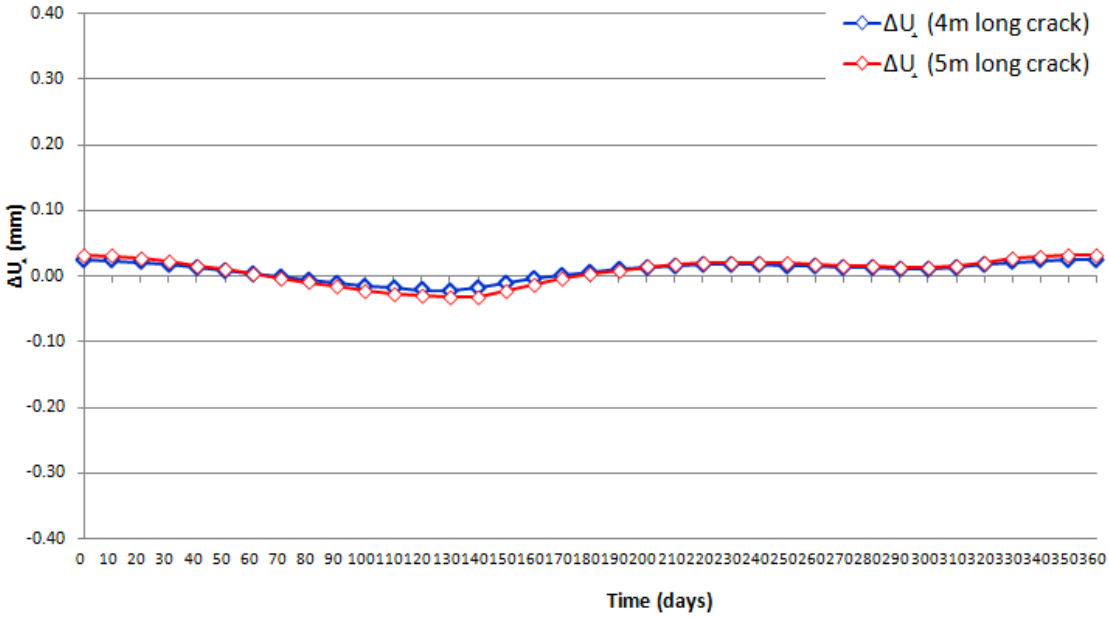


**Figure 45. Computed crack opening displacements perpendicularly to the downstream surface of the dam**

According to **Figure 45,** negligible opening displacements are taking place perpendicularly to the dam downstream surface. Therefore, the crack is opening in the direction parallel to the dam surface only. This can be due to the fact that the crack has been modelled considering frictionless contact and its direction of propagation is almost perpendicular to the dam downstream face.

# 4. Conclusions

In the course of construction and particularly during the service period, it is necessary to perform continuous monitoring and surveillance of the concrete dam in order to have permanent insight into the condition and behaviour of the structure, enabling timely anticipation of any possible threat to its safety. Visual inspection, traditional instruments, instruments embedded in the structure for joints opening displacement measurements, as well as special methods as Ground-Based radar Interferometry with Synthetic Aperture Radar (GB InSAR) technique, Terrestrial Laser Scanning (TLS) and Digital Image Correlation (DIC) are addressed herein, together with their basic principles and concepts. A case study is presented, in which a 2D finite element (FE) analysis investigating the effects of the crack propagation on the deformation behaviour of the block characterised by the tallest cross section of the Chencun arch-gravity dam is performed. A transient thermal analysis and a linear elastic static analysis are carried out. The results of the thermal analysis show that water temperature is more effective than air temperature in the temperature distribution of the dam across the thickness. The computed upstream-downstream (UD) crest displacements of the dam block, subjected to thermal load only and considering 4 and 5 meter long cracks, show a regular behaviour of the responses under temperature fluctuation. Furthermore, the propagation of the crack leads to an amplitude decrease of UD crest displacements. The annual variations of the deflection curve of the dam block show that the crack propagation leads to an amplitude decrease of UD displacements for the upper part of the dam only, while, for elevations lower than the one of the crack, the annual variations of the deflection curves are almost equivalent before and after the crack further propagation. As of crack opening, during the months characterised by higher temperatures (from May to October), the crack closes, while during the colder months (from November to April), the crack opens. The crack further propagation lead to an amplitude increase of the crack opening displacements in the direction parallel to the downstream face of the dam. On the other hand, the magnitude of the opening displacements in the perpendicular direction can provide an indication of the direction of propagation of the crack, in the case in which the crack is modelled considering frictionless contact. In the considered case study, the latter displacements are negligible, since the crack propagates almost perpendicularly to the dam downstream face.

# 5. References


[1] Maier, Giulio & Ardito, Raffaele & Fedele, Roberto. (2004). Inverse analysis problems in structural engineering of concrete dams. 9.

[2] Dams and Appurtenant Hydraulic Structures, Ljubomir Tanchev, 2nd Edition, 2014

[3] Hu, Jiang & Wu, Suhua. (2018). Statistical modeling for deformation analysis of concrete arch dams with influential horizontal cracks. Structural Health Monitoring. 18. 147592171876030. 10.1177/1475921718760309.

[4] Wieland, Martin & F. Kirchen, G. (2012). Long-term dam safety monitoring of Punt dal Gall arch dam in Switzerland. Frontiers of Structural and Civil Engineering. 6. 10.1007/s11709-012-0144-z.

[5] Human, Odon & Oosthuizen, C. (2016). NOTES ON THE BEHAVIOUR OF A 65 YEAR OLD CONCRETE ARCH DAM AFFECTED BY AAR (MAINLY BASED ON VISUAL OBSERVATIONS).

[6] Campos, André & López, Carlos & Blanco, Ana & Aguado, Antonio. (2016). Structural Diagnosis of a Concrete Dam with Cracking and High Nonrecoverable Displacements. Journal of Performance of Constructed Facilities. 30. 10.1061/(ASCE)CF.1943-5509.0000869.

[7] Luo, Danni & Lin, Peng & Li, Qingbin & Zheng, Dong & Liu, Hongyuan. (2015). Effect of the impounding process on the overall stability of a high arch dam: a case study of the Xiluodu dam, China. Arabian Journal of Geosciences. 8. 10.1007/s12517-015-1868-6.

[8] Hua Cui, Jian & Jiang Xiao, Han & Shan, Liang. (2011). Contact Analysis on the Longitudinal Joint of Gravity Dam. Advanced Materials Research. 250-253. 2931-2934. 10.4028/www.scientific.net/AMR.250-253.2931.

[9] Bukenya, Patrick. (2014). Health monitoring of concrete dams: a literature review. Journal of Civil Structural Health Monitoring.

[10] Willm G and Beaujoint N. Les me´thodes de surveillance des barrages au service de la production hydraulique d'Electricite´ de France-Proble`mes anciens et solutions nouvelles. In: International Commission on Large Dams (ICOLD), 9th Congress on large dams, vol. III, Istanbul, Turkey, 1967, pp.529–550. (in French).

[11] Berberan, Antonio & Portela, Eliane & Boavida, João. (2006). Assisted visual inspection of dams as a tool for structural safety control. A case study..

[12] Alba, Mario & Bernardini, Giulia & Giussani, Alberto & Paolo Ricci, Pier & Roncoroni, Fabio & Scaioni, Marco & Valgoi, Paolo & Zhang, Katherine. (2008). Measurement of dam deformations by terrestrial interferometric techiques. International Archives of Photogrammetry, Remote Sensing and Spatial Information Sciences. 37.

[13] Strumenti e metodi per il monitoraggio delle strutture e dei fenomeni. Alberto Giussani. Politecnico di Milano. AUTeC 2007. GEOMATICA. La didattica all'inseguimento dell'evoluzione scientifica e tecnologica. Cosa insegnare. Come insegnare. Pavia, 10-11 Maggio 2007.

[14] Chouinard, Luc & Roy, Vincnet. (2015). PERFORMANCE OF STATISTICAL MODELS FOR DAM MONITORING DATA.

[15] Kaamin, Masiri & Azyyati Idris, Noor & MOHD BUKARI, SAIFULLIZAN & Ali, Zaurin & Samion, Norhafiza & A. A., Mustaffa. (2017). Visual Inspection of Historical Buildings Using Micro UAV. MATEC Web of Conferences. 103. 07003. 10.1051/matecconf/201710307003.

[16] De Sortis, Adriano & Paoliani, P. (2007). Statistical analysis and structural identification in concrete dam monitoring. Engineering Structures - ENG STRUCT. 29. 110-120. 10.1016/ j.engstruct. 2006.04.022.

[17] Fedele, Roberto & Maier, G & Miller, B. (2006). Health Assessment of Concrete Dams by Overall Inverse Analyses and Neural Networks. International Journal of Fracture. 137. 151-172. 10.1007/s10704-006-6582-7.

[18] Ferdinand Klug, Werner Lienhart and Helmut Woschitz. High resolution monitoring of expansion joints of a concrete arch dam using fiber optic sensors*. Proc. 6th World Conference on Structural Control and Monitoring (6WCSCM), 2014, Barcelona, Spain: 3164-3176

[19] www.geosense.co.uk

[20] www.berntsen.com

[21] Zac James Prins. INVESTIGATING THE OPERATIONAL BEHAVIOUR OF A DOUBLE CURVATURE ARCH DAM. FACULTY OF ENGINEERING AND THE BUILT ENVIRONMENT DEPARTMENT OF CIVIL ENGINEERING.

[22] Milan Talich. The Deformation Monitoring of Dams by the Ground-Based InSAR Technique - Case Study of Concrete Hydropower Dam

Orlík.Int'l Journal of Advances in Agricultural & Environmental Engg. (IJAAEE) Vol. 3, Issue 1 (2016) ISSN 2349-1523 EISSN 2349-1531

[23] Ardito, Raffaele & Cocchetti, Giuseppe. (2006). Statistical approach to damage diagnosis of concrete dams by radar monitoring: Formulation and a pseudo-experimental test. Engineering Structures. 28. 2036-2045. 10.1016/j.engstruct.2006.04.001.

[24] Pan, Bing & Qian, Kemao & Xie, Huimin & Asundi, Anand. (2009). TOPICAL REVIEW: Two-dimensional digital image correlation for in-plane displacement and strain measurement: a review. Measurement Science & Technology - MEAS SCI TECHNOL. 20. 10.1088/0957-0233/20/6/062001.

[25] Reagan, Daniel & Sabato, Alessandro & Niezrecki, Christopher. (2017). Unmanned aerial vehicle acquisition of three-dimensional digital image correlation measurements for structural health monitoring of bridges. 1016909. 10.1117/12.2259985.

[26] Colombo, Martina & Domaneschi, Marco & Ghisi, Aldo. (2016). Existing concrete dams: Loads definition and finite element models validation. Structural Monitoring and Maintenance. Vol. 3. 129-144. 10.12989/smm.2016.3.2.129.

[27] Andreini, Marco & De Falco, Anna & Marmo, Giovanni & Mori, Matteo & Sevieri, Giacomo. (2017). Modelling issues in the structural analysis of existing concrete gravity dams.

[28] Qingbin Li, Guohe Liang, Yu Hu, and Zheng Zuo, "Numerical Analysis on Temperature Rise of a Concrete Arch Dam after Sealing Based on Measured Data," Mathematical Problems in Engineering, vol. 2014, Article ID 602818, 12 pages, 2014. https: //doi.org/ 10.1155/ 2014/ 602818.

[29] Bofang, Z. _1997_. "Prediction of water temperature in deep reservoir."Dam Eng., VIII_1_, 13–25.

[30] Sheibani, Farrokh & Ghaemian, Mohsen. (2006). Effects of Environmental Action on Thermal Stress Analysis of Karaj Concrete Arch Dam. Journal of Engineering Mechanics-asce - J ENG MECH-ASCE. 132. 10.1061/(ASCE)0733-9399(2006)132:5(532).